A numerical study of low Reynolds number slip flow in the hydrodynamic development region of circular and parallel plate ducts

R. W. Barber and D. R. Emerson

Centre for Microfluidics,
Department of Computational Science and Engineering,
CLRC Daresbury Laboratory,
Daresbury,
Warrington,
WA4 4AD.

Abstract

One of the major difficulties in trying to predict gaseous transport in micron-sized devices can be attributed to the fact that the continuum flow assumption implemented in the Navier-Stokes equations breaks down when the mean free path of the molecules is comparable to the characteristic dimensions of the flow domain. Under these conditions, the momentum transfer starts to be affected by the discrete molecular composition of the gas and a variety of non-continuum or rarefaction effects are likely to be exhibited. Velocity profiles, volume rates of flow and boundary wall shear stresses are all influenced by the non-continuum regime. In addition, the length of the hydrodynamic development region at the entrance to a channel may also be affected.

The present investigation examines the effects of the Reynolds number and the Knudsen number on the hydrodynamic development lengths in circular and parallel plate ducts. The study was conducted using THOR-2D – a two-dimensional finite-volume Navier-Stokes solver developed by the Computational Engineering Group at CLRC Daresbury Laboratory. The solver was specifically adapted for the simulation of non-continuum flows by the inclusion of appropriate tangential slip-velocity boundary conditions at the solid perimeter walls. Results from the present study suggest that hydrodynamic development lengths for the circular pipe are only marginally affected by Knudsen number. However, in the case of the parallel plate geometry, entrance development lengths in the slip-flow regime are approximately 25% longer than the corresponding continuum solution.

Contents

1 Introduction

The analysis of flow development in the hydrodynamic entrance region of circular and rectangular ducts has received considerable attention over the years. An analytical solution of the complete non-linear Navier-Stokes equations is not feasible in the entrance region and therefore early solutions of the problem often employed approximations of Prandtl's boundary layer equations. For example, Schlichting [1,2] proposed a series expansion technique to analyse the flow development in a two-dimensional channel. The method consisted of smoothly blending two asymptotic series expansions for the flow, one based upon Blasius' solution of boundary-layer development, expanded in the downstream direction, and the other based upon the parabolic Hagen-Poiseuille velocity distribution, expanded upstream towards the entrance. By patching the two series expansions together, Schlichting was able to produce a flow solution for any intermediate location in the entrance region. A similar methodology was also employed by Atkinson & Goldstein [3] to analyse the flow development in a circular pipe. Davies [4] and Van Dyke [5] subsequently refined Schlichting's method by including higher order terms in the expansions.

Alternatively, other researchers have chosen to linearise the inertia terms in the Navier-Stokes equations in order to formulate an analytical solution. For example, Langhaar [6] proposed two simplifying assumptions to obtain a tractable solution; namely, that the pressure can be assumed constant over a given cross-section (i.e. $\partial p / \partial y = 0$) and that the $v\,\partial u / \partial y$ term in the axial-direction Navier-Stokes equation can be neglected. Although these assumptions permit an analytical solution, they are not necessarily valid in the near-entrance region. Lundgren *et al*. [7] employed a comparable linearisation technique to predict the pressure drop in the entrance region of ducts of arbitrary cross-section whilst Han [8] used a similar methodology to produce an analytical solution for flow development in a three-dimensional rectangular duct.

In addition to the analytical techniques outlined above, numerous authors have employed numerical simulations to investigate the same problem. One of the first studies was conducted by Bodoia & Osterle [9] who utilised a finite-difference method to solve Prandtl's boundary-layer equations. Wang & Longwell [10] later presented an alternative streamfunction/vorticity-transport model of the complete Navier-Stokes equations for the inlet region between parallel plates. Friedmann *et al*. [11] subsequently modified Wang & Longwell's method and applied it to the entrance region of a circular pipe. In addition, Atkinson *et al*. [12] analysed the hydrodynamic development lengths in pipes and channels under creeping flow conditions using a finite-element method. Other notable authors include Morihara & Cheng [13] who employed a primitive variable solution methodology for the parallel plate geometry and Chen [14] who presented a novel numerical solution for the momentum integral equations.

Whilst most researchers have concentrated their efforts on the no-slip flow regime, several authors have investigated the hydrodynamic entrance problem under slip flow conditions where the momentum transport starts to be affected by the discrete molecular composition of the fluid. For example, Sparrow *et al*. [15] and Ebert & Sparrow [16] formulated analytical slip flow solutions for rectangular and

annular ducts, Sreekanth [17] developed an analytical solution for the pressure drop in circular pipes, whilst Quarmby [18] and Gampert [19] used finite-difference simulations to investigate developing slip flow in circular pipes and parallel plates.

Until recently, non-continuum slip flows were only encountered in low-density (rarefied gas) applications such as vacuum or space-vehicle technology. However, the rapid progress in fabricating and utilising Micro Electro Mechanical Systems (MEMS) over the last decade [20,21,22] has led to considerable interest in non-continuum flow processes (Beskok *et al.* [23,24]). The small length scales commonly encountered in MEMS imply that rarefaction effects occur in micron-sized channels at normal operating pressures. For example, the mean free path of air molecules at SATP (standard ambient temperature and pressure) is approximately 70 nm (see Appendix C). Consequently, the ratio of the mean free path of the gas molecules to the characteristic dimensions of a MEMS device can be appreciable. This ratio is referred to as the Knudsen number and as it increases, the gas begins to exhibit non-continuum effects. It is therefore imperative that the designer of a microfluidic device understands the unconventional transport phenomena associated with the non-continuum flow regime.

The present study is designed to examine the effects of both the Reynolds number and the Knudsen number on the hydrodynamic development length at the entrance to circular pipes and parallel plates. The circular pipe is important not only because of its fundamental geometrical properties but also because gas samples are commonly transported to MEMS devices in fine-bore micro-capillary tubing. The second study concerned with the parallel plate geometry is equally important as it forms the limiting flow condition for large aspect ratio rectangular ducts commonly encountered in silicon-based microfluidic devices (Pfahler *et al*. [25], Harley *et al*. [26], Arkilic *et al*. [27-30]).

2 Governing hydrodynamic equations

The Navier-Stokes equations governing the flow of a viscous, laminar, Newtonian fluid of constant viscosity can be written in tensor notation as follows:
continuity:

$$\frac{\partial \rho}{\partial t} + \frac{\partial (\rho u_k)}{\partial x_k} = 0 \tag{1}$$

momentum:

$$\frac{\partial (\rho u_i)}{\partial t} + \frac{\partial (\rho u_k u_i)}{\partial x_k} = -\frac{\partial p}{\partial x_i} + \frac{\partial \tau_{ik}}{\partial x_k} \tag{2}$$

where u is the velocity, p is the pressure and ρ is the fluid density. τ_{ij} is the viscous stress tensor given by

$$\tau_{ij} = \mu \left(\frac{\partial u_i}{\partial x_j} + \frac{\partial u_j}{\partial x_i} \right) - \frac{2}{3} \mu \frac{\partial u_k}{\partial x_k} \delta_{ij} \tag{3}$$

where μ is the coefficient of dynamic viscosity and δ_{ij} is the Kronecker delta.

For a two-dimensional flow in a Cartesian (x,y) co-ordinate system, the above equations can be expressed as

continuity:

$$\frac{\partial \rho}{\partial t}+\frac{\partial(\rho u)}{\partial x}+\frac{\partial(\rho v)}{\partial y}=0 \tag{4}$$

x-momentum:

$$\begin{aligned}\frac{\partial(\rho u)}{\partial t}+\frac{\partial(\rho u u)}{\partial x}+\frac{\partial(\rho u v)}{\partial y}-\frac{\partial}{\partial x}\left(\mu\frac{\partial u}{\partial x}\right)-\frac{\partial}{\partial y}\left(\mu\frac{\partial u}{\partial y}\right)= \\ -\frac{\partial}{\partial x}\left(p+\frac{2}{3}\mu\nabla.\mathbf{V}\right)+\frac{\partial}{\partial x}\left(\mu\frac{\partial u}{\partial x}\right)+\frac{\partial}{\partial y}\left(\mu\frac{\partial v}{\partial x}\right)\end{aligned} \tag{5}$$

y-momentum:

$$\begin{aligned}\frac{\partial(\rho v)}{\partial t}+\frac{\partial(\rho u v)}{\partial x}+\frac{\partial(\rho v v)}{\partial y}-\frac{\partial}{\partial x}\left(\mu\frac{\partial v}{\partial x}\right)-\frac{\partial}{\partial y}\left(\mu\frac{\partial v}{\partial y}\right)= \\ -\frac{\partial}{\partial y}\left(p+\frac{2}{3}\mu\nabla.\mathbf{V}\right)+\frac{\partial}{\partial x}\left(\mu\frac{\partial u}{\partial y}\right)+\frac{\partial}{\partial y}\left(\mu\frac{\partial v}{\partial y}\right)\end{aligned} \tag{6}$$

where u is the velocity component in the x-direction, v is the velocity component in the y-direction and the divergence of the velocity field in eqns. (5) & (6) is given by

$$\nabla.\mathbf{V}=\frac{\partial u}{\partial x}+\frac{\partial v}{\partial y} \tag{7}$$

Alternatively, in the case of two-dimensional axisymmetric flow in a cylindrical co-ordinate system, the Navier-Stokes equations can be expressed as

continuity:

$$\frac{\partial \rho}{\partial t}+\frac{\partial(\rho u)}{\partial x}+\frac{1}{r}\frac{\partial(\rho r v)}{\partial r}=0 \tag{8}$$

x-momentum:

$$\begin{aligned}\frac{\partial(\rho u)}{\partial t}+\frac{\partial(\rho u u)}{\partial x}+\frac{1}{r}\frac{\partial(\rho r u v)}{\partial r}-\frac{\partial}{\partial x}\left(\mu\frac{\partial u}{\partial x}\right)-\frac{1}{r}\frac{\partial}{\partial r}\left(r\mu\frac{\partial u}{\partial r}\right)= \\ -\frac{\partial}{\partial x}\left(p+\frac{2}{3}\mu\nabla.\mathbf{V}\right)+\frac{\partial}{\partial x}\left(\mu\frac{\partial u}{\partial x}\right)+\frac{1}{r}\frac{\partial}{\partial r}\left(r\mu\frac{\partial v}{\partial x}\right)\end{aligned} \tag{9}$$

and

r-momentum:

$$\frac{\partial(\rho v)}{\partial t}+\frac{\partial(\rho u v)}{\partial x}+\frac{1}{r}\frac{\partial(\rho r v v)}{\partial r}-\frac{\partial}{\partial x}\left(\mu\frac{\partial v}{\partial x}\right)-\frac{1}{r}\frac{\partial}{\partial r}\left(r\mu\frac{\partial v}{\partial r}\right)= \\ -\frac{\partial}{\partial r}\left(p+\frac{2}{3}\mu\nabla.\mathbf{V}\right)+\frac{\partial}{\partial x}\left(\mu\frac{\partial u}{\partial r}\right)+\frac{1}{r}\frac{\partial}{\partial r}\left(r\mu\frac{\partial v}{\partial r}\right)-\frac{2\mu v}{r^2} \tag{10}$$

where u is the velocity component in the x-direction and v is the velocity component in the r-direction. The divergence of the velocity field in cylindrical co-ordinates is given by

$$\nabla.\mathbf{V}=\frac{\partial u}{\partial x}+\frac{1}{r}\frac{\partial(r v)}{\partial r} \tag{11}$$

3 Slip-velocity boundary conditions

To account for non-continuum flow effects, the Navier-Stokes equations are solved in conjunction with the slip-velocity boundary condition proposed by Basset [31]:

$$\tau_t=\beta u_t \tag{12}$$

where u_t is the tangential slip-velocity at the wall, τ_t is the tangential shear stress on the wall and β is the slip coefficient. Schaaf & Chambre [32] show that the slip coefficient can be related to the mean free path of the molecules as follows:

$$\beta=\frac{\mu}{\left(\frac{2-\sigma}{\sigma}\right)\lambda} \tag{13}$$

where μ is the viscosity of the gas, σ is the tangential momentum accommodation coefficient (TMAC) and λ is the mean free path. For an idealised wall (perfectly smooth at the molecular level), the angles of incidence and reflection of molecules colliding with the wall are identical and therefore the molecules conserve their tangential momentum. This is referred to as *specular reflection* and results in perfect slip at the boundary. Conversely, in the case of an extremely rough wall, the molecules are reflected at a totally random angle and lose all their tangential momentum (referred to as *diffusive reflection*). For real walls, some molecules will reflect diffusively and some will reflect specularly, and therefore the tangential momentum accommodation coefficient, σ, is introduced to account for the momentum retained by the molecules. Theoretically, the coefficient lies between 0 and 1 and is defined as the fraction of molecules reflected diffusively. The value of σ depends upon the particular solid and gas involved and the surface finish of the wall. TMAC values lying in the range 0.2 to 1.0 have been determined experimentally by Thomas & Lord [33] and Arkilic *et al*. [34].

Equations (12) and (13) can be combined and rearranged to give

$$u_t = \frac{2-\sigma}{\sigma}\frac{\lambda}{\mu}\tau_t \tag{14}$$

It is convenient at this stage to recast the mean free path in eqn. (14) in terms of a non-dimensionalised Knudsen number, *Kn*. The choice of the characteristic length scale utilised in the definition of the Knudsen number depends upon the flow geometry under consideration. In the case of a circular pipe, it is convenient to specify the diameter as the appropriate length scale since this is then compatible with the definition of the Reynolds number. Thus, the Knudsen number, *Kn*, is defined as the ratio of the mean free path of the gas molecules, λ, to the diameter of the pipe, D:

$$Kn = \frac{\lambda}{D} \tag{15}$$

Consequently, eqn. (14) can be rewritten as

$$u_t = \frac{2-\sigma}{\sigma}\frac{Kn\,D}{\mu}\tau_t \tag{16}$$

The shear stress on the pipe wall ($r = R$) is then expressed in terms of the local velocity gradient:

$$\tau_t = -\mu\left.\frac{\partial u}{\partial r}\right|_{r=R} \tag{17}$$

The negative sign is introduced into the above expression to account for the fact that the velocity gradient, $\partial u/\partial r$ is negative. Substituting eqn. (17) into (16) then yields the tangential slip-velocity:

$$u_t = -\frac{2-\sigma}{\sigma}Kn\,D\left.\frac{\partial u}{\partial r}\right|_{r=R} \tag{18}$$

In the case of non-circular ducts, the Reynolds number is traditionally defined in terms of the *hydraulic diameter*, D_h (see Schlichting [1], Shah & London [35] or White [36]):

$$D_h = \frac{4\times\text{area}}{\text{wetted perimeter}} = \frac{4A}{P} \tag{19}$$

For the specific case of flow between parallel plates separated by a distance, *H*, it can readily be shown that the hydraulic diameter equals twice the plate separation, i.e.

$$D_h = 2H \tag{20}$$

Consequently, the Knudsen number, *Kn*, is defined as the ratio of the mean free path

of the gas molecules, λ, to the hydraulic diameter of the duct, D_h:

$$Kn = \frac{\lambda}{D_h} = \frac{\lambda}{2H} \tag{21}$$

As an aside, it should be noted that the earlier definition of Knudsen number for a circular pipe (eqn. 15) is consistent with the present definition since $D_h = D$ for circular cross-sections.

Substituting eqn. (21) into (14), allows the tangential slip-velocity at the wall to be written in terms of the Knudsen number:

$$u_t = \frac{2-\sigma}{\sigma} \frac{Kn\, 2H}{\mu} \tau_t \tag{22}$$

The shear stress on the upper wall of the duct ($y = H$) is then related to the local velocity gradient as follows:

$$\tau_t = -\mu \left. \frac{\partial u}{\partial y} \right|_{y=H} \tag{23}$$

Substituting eqn. (23) into (22) finally yields the tangential slip-velocity:

$$u_t = -\frac{2-\sigma}{\sigma} Kn\, 2H \left. \frac{\partial u}{\partial y} \right|_{y=H} \tag{24}$$

The governing hydrodynamic equations were solved using THOR-2D – a two-dimensional finite-volume Navier-Stokes solver developed by the Computational Engineering Group at CLRC Daresbury Laboratory [37]. Additional subroutines were specifically written to account for the slip-velocity boundary conditions at the solid perimeter walls (eqns. 18 & 24). Since the flows investigated in the present study had relatively low Mach numbers, compressibility effects were ignored and the flow was therefore considered to be incompressible.

4 Estimation of hydrodynamic development lengths

When a viscous fluid enters a duct, the uniform velocity distribution at the entrance is gradually redistributed towards the centreline due to the retarding influence of the shear stresses along the side walls. Ultimately, the flow will reach a location where the velocity profile no longer changes in the axial-direction, and under such conditions the flow is said to be *fully-developed*. Theoretically, the required distance to reach the fully-developed solution is infinitely large. However, for practical engineering calculations, the *hydrodynamic development length* is arbitrarily defined as the axial distance required for the maximum velocity in the duct to attain a value of 99% of the corresponding fully-developed maximum velocity.

Several authors have chosen to base the 99% velocity cut-off point in terms of the *numerically predicted* fully-developed profile at the outflow boundary. This has the advantage that the fully-developed profile does not have to be known *a priori* which may be important for ducts of arbitrary cross-section. However, the regular geometries considered in the present study permit analytical solutions of the Navier-Stokes equations and therefore exact expressions for the fully-developed velocity profiles can be obtained.

In the case of laminar slip flow in a circular pipe, it can be shown (Appendix A) that the maximum velocity at the centreline is given by

$$u_{\max} = 2\overline{u}\,\frac{\left(1+4\dfrac{2-\sigma}{\sigma}Kn\right)}{\left(1+8\dfrac{2-\sigma}{\sigma}Kn\right)} \tag{25}$$

where $\overline{u}$ is the mean or average velocity in the pipe and σ is the tangential momentum accommodation coefficient. As an aside, in the limit of $Kn \to 0$ (i.e. the continuum flow regime), eqn. (25) yields the familiar no-slip (NS) solution given by Hagen-Poiseuille pipe theory:

$$u_{\max(\mathrm{NS})} = 2\overline{u} \tag{26}$$

Using eqn. (25) in conjunction with the 99% velocity cut-off rule then allows the hydrodynamic development length to be defined as the location where the longitudinal velocity at the centreline of the pipe reaches a value of

$$u = 1.98\ \overline{u}\,\frac{\left(1+4\dfrac{2-\sigma}{\sigma}Kn\right)}{\left(1+8\dfrac{2-\sigma}{\sigma}Kn\right)} \tag{27}$$

In order to determine the hydrodynamic development length, interpolation has to be used to estimate the velocity variation between grid nodes along the centreline of the pipe.

For the case of non-continuum slip flow between parallel plates, it can be shown (Appendix B) that the maximum velocity at the centre of the duct is given by

$$u_{\max} = \frac{3}{2}\overline{u}\,\frac{\left(1+8\dfrac{2-\sigma}{\sigma}Kn\right)}{\left(1+12\dfrac{2-\sigma}{\sigma}Kn\right)} \tag{28}$$

Furthermore, in the limit of $Kn \to 0$, eqn. (28) yields the familiar no-slip solution:

$$u_{\max(\mathrm{NS})} = \frac{3}{2}\bar{u} \tag{29}$$

Using an analogous 99% velocity cut-off procedure to that employed for the circular pipe then allows the hydrodynamic development length to be defined as the location where the longitudinal velocity at the centreline of the duct reaches a value of

$$u = 1.485\ \bar{u}\,\frac{\left(1+8\frac{2-\sigma}{\sigma}Kn\right)}{\left(1+12\frac{2-\sigma}{\sigma}Kn\right)} \tag{30}$$

5 Boundary conditions

5.1 *Circular pipe geometry*

The imposed boundary conditions for the circular pipe geometry are detailed schematically in Figure 1. It should be noted that the problem has been non-dimensionalised and therefore the uniform velocity at the entrance to the duct, the density of the fluid and the diameter of the pipe are taken as unity. With reference to Figure 1, the four boundaries of the pipe are treated as follows:

(a) *Entrance boundary:*
The velocity distribution at the entrance is assumed to be uniform and parallel to the longitudinal axis of the pipe, i.e.

$$u = 1 \quad \text{and} \quad v = 0 \qquad \text{at} \quad x = 0\ ,\ 0 \le \mathrm{r} \le \mathrm{R} \tag{31}$$

(b) *Wall boundary:*
The tangential slip-velocity along the wall of the pipe is evaluated using eqn. (18) as detailed in Section 3. In addition, there must be zero normal flow across the wall. Hence,

$$u = -\frac{2-\sigma}{\sigma}Kn\,D\left.\frac{\partial u}{\partial r}\right|_{r=R} \quad \text{and} \quad v = 0 \qquad \text{at} \quad r = R\ ,\ 0 \le x \le l \tag{32}$$

where l is the total length of the duct.

(c) *Centreline boundary:*
The flow must be symmetrical about the centreline of the pipe:

$$\frac{\partial u}{\partial r} = 0 \quad \text{and} \quad v = 0 \qquad \text{at} \quad r = 0\ ,\ 0 \le x \le l \tag{33}$$

(d) *Outflow boundary:*
The flow should approach the fully-developed solution at the downstream boundary and consequently the gradients of the flow variables in the axial-direction must tend to zero, i.e.

$$\frac{\partial u}{\partial x} = 0 \quad \text{and} \quad \frac{\partial v}{\partial x} = 0 \qquad \text{at} \quad x = l \ , \ 0 \le r \le R \tag{34}$$

5.2 *Parallel plate geometry*

The imposed boundary conditions for the parallel plate geometry are detailed in Figure 2. To reduce the computational costs of the numerical simulation, the analysis makes use of the implicit flow symmetry about the mid-plane of the duct and consequently only the upper half-plane is considered. The four separate boundaries are therefore specified as follows:

(a) *Entrance boundary:*
The velocity distribution at the entrance of the duct is assumed to be uniform and parallel to the longitudinal axis, i.e.

$$u = 1 \quad \text{and} \quad v = 0 \qquad \text{at} \quad x = 0 \ , \ \frac{H}{2} \le y \le H \tag{35}$$

(b) *Wall boundary:*
The tangential slip-velocity along the upper wall of the duct is evaluated using eqn. (24) as detailed in Section 3. In addition, there must be zero normal flow across the wall. Hence,

$$u = -\frac{2-\sigma}{\sigma} Kn \, 2H \left.\frac{\partial u}{\partial y}\right|_{y=H} \quad \text{and} \quad v = 0 \qquad \text{at} \quad y = H \ , \ 0 \le x \le l \tag{36}$$

(c) *Centreline boundary:*
The flow must be symmetrical about the centreline of the duct:

$$\frac{\partial u}{\partial y} = 0 \quad \text{and} \quad v = 0 \qquad \text{at} \quad y = \frac{H}{2} \ , \ 0 \le x \le l \tag{37}$$

(d) *Outflow boundary:*
The flow should approach the fully-developed solution at the downstream boundary and consequently the gradients of the flow variables in the axial-direction must tend to zero, i.e.

$$\frac{\partial u}{\partial x} = 0 \quad \text{and} \quad \frac{\partial v}{\partial x} = 0 \qquad \text{at} \quad x = l \ , \ \frac{H}{2} \le y \le H \tag{38}$$

6 Numerical results

The numerical simulations assessed the entrance development lengths for a range of different Reynolds and Knudsen numbers. In the present series of tests, the Reynolds number was varied from *Re*=1 to *Re*=400 whilst the Knudsen number was varied from *Kn*=0 (continuum flow) to *Kn*=0.1 (a frequently adopted upper bound for the slip-flow regime). The tangential momentum accommodation coefficient, σ, was assumed to have a value of unity in all computations. To avoid confusion in interpreting the results, it should be remembered that both the Reynolds and Knudsen numbers are defined using the *hydraulic diameter* as the characteristic length scale. Thus, in the case of the circular pipe:

$$Re = \frac{\rho \bar{u} D}{\mu} \qquad \text{and} \qquad Kn = \frac{\lambda}{D} \tag{39}$$

whilst for the parallel plate geometry:

$$Re = \frac{\rho \bar{u} 2H}{\mu} \qquad \text{and} \qquad Kn = \frac{\lambda}{2H} \tag{40}$$

The tests involved a number of different grid resolutions, including meshes composed of 51×21, 101×41 and 201×101 nodes. As detailed later, grid independent results were judged to have been achieved using the intermediate 101x41 mesh. In addition, numerical experimentation was used to decide upon a suitable length of duct, *l*. Ideally, a co-ordinate transformation which maps the downstream boundary to infinity should be employed (see Morihara & Cheng [13]) but it was found that this resulted in numerical instabilities which were thought to arise from the extremely large grid aspect ratios close to the outflow. Consequently, the meshes were curtailed at a finite distance downstream of the entrance, with the location chosen so as not to affect the estimation of the hydrodynamic development lengths. In the present study (with Reynolds numbers up to 400), it was found that duct lengths of $l = 40D$ for the circular pipe and $l = 20D_h$ for the parallel plate geometry were sufficient to achieve a reliable estimation of the hydrodynamic development lengths. In addition, an exponential stretching of the meshes in the axial-direction was implemented to achieve a finer grid resolution in the critical boundary-layer formation zone at the entrance to the ducts. The exponential stretching was chosen so that the grid aspect ratio ($\Delta x/\Delta r$ or $\Delta x/\Delta y$) varied from unity at the entrance up to approximately 120 at the outflow (the upper bound of 120 preventing the occurrence of numerical instabilities). All simulations relied upon the implicit flow symmetry about the centreline and therefore the numerical computations only considered the upper half-plane of each duct. However, for presentational purposes, the remainder of the flow domain was "reconstructed" to obtain the entire velocity profile.

6.1 *Numerical validation*

Preliminary validation of the hydrodynamic code was accomplished by comparing numerical and analytical fully-developed velocity profiles for each geometry. In the case of laminar slip flow in a circular pipe, it can be shown (Appendix A) that the theoretical velocity profile is given by

$$u(r) = 2\overline{u}\,\frac{\left(1-\frac{r^2}{R^2}+4\frac{2-\sigma}{\sigma}Kn\right)}{\left(1+8\frac{2-\sigma}{\sigma}Kn\right)} \tag{41}$$

In the limit of $Kn \to 0$ (continuum flow), eqn. (41) reverts to the familiar no-slip (NS) solution given by Hagen-Poiseuille pipe theory:

$$u_{\mathrm{NS}}(r) = 2\overline{u}\left(1-\frac{r^2}{R^2}\right) \tag{42}$$

Similarly, for laminar slip flow between parallel plates, it can be shown (Appendix B) that the velocity profile across the duct is given by

$$u(y) = 6\overline{u}\,\frac{\left(\frac{y}{H}-\frac{y^2}{H^2}+2\frac{2-\sigma}{\sigma}Kn\right)}{\left(1+12\frac{2-\sigma}{\sigma}Kn\right)} \tag{43}$$

and therefore in the limit of $Kn \to 0$, eqn. (43) reverts to the familiar no-slip solution:

$$u_{\mathrm{NS}}(y) = 6\overline{u}\left(\frac{y}{H}-\frac{y^2}{H^2}\right) \tag{44}$$

The validation tests compared the analytical velocity profiles given in eqns. (41) & (43) against predictions from the downstream boundary of the numerical model. Three separate Knudsen numbers ($Kn = 0$, 0.05 and 0.10) were considered and the Reynolds number for the numerical simulations was set to its highest value ($Re = 400$). Choosing to run the tests at the highest Reynolds number (longest hydrodynamic development length) allowed an immediate assessment of the suitability of the hydrodynamic mesh. If a chosen mesh had insufficient length to allow full development of the velocity profile, the numerical predictions would have shown obvious discrepancies against the analytical solution.

The results for the circular pipe and parallel plate geometry are presented in non-dimensionalised form in Figures 3 & 4. Both sets of velocity profiles show excellent agreement between the numerical and analytical solutions, clearly validating the hydrodynamic model. Slight discrepancies can be seen at the centreline of the

circular pipe for a Knudsen number, $Kn = 0$, but the maximum error amounts to less than 0.15%.

Figures 3 & 4 also provide a useful visualisation of the changes which take place in the velocity profile as non-continuum flow effects start to dominate. It can be seen that as the Knudsen number increases, the maximum velocity at the centre of the duct decreases whilst the tangential slip-velocity at the wall increases. The net effect of these changes is to produce a velocity profile which becomes more uniform with increasing Knudsen number. Another interesting feature of the flow redistribution is the fact that the velocity remains invariant with respect to Knudsen number at two locations across the duct. It can readily be shown that for the circular pipe, the position of this feature occurs at

$$\frac{r}{D} = \pm \frac{1}{2\sqrt{2}} \tag{45}$$

whilst for flow between parallel plates, the feature occurs at

$$\frac{y}{H} = \frac{1}{2} \pm \frac{1}{2\sqrt{3}} \tag{46}$$

6.2 *Hydrodynamic development lengths*

After validating the hydrodynamic code against the analytical fully-developed velocity profiles, the numerical model was then used to examine the effects of the Reynolds number and the Knudsen number on the entrance development length. As previously described in Section 4, the computations for the entrance length were based upon the 99% velocity cut-off point.

6.2.1 *Circular pipe*

Tables 1 & 2 present non-dimensionalised hydrodynamic development lengths (*L/D*) for three separate Knudsen numbers ($Kn = 0$, 0.05 and 0.10) and a range of Reynolds numbers between 1 and 400. The results in Table 1 were evaluated using a 101×41 hydrodynamic mesh whilst the results in Table 2 employed a much higher resolution 201×101 mesh. The computed hydrodynamic development lengths for the two grid resolutions were found to be very similar and consequently mesh independent results were judged to be achieved using the 101×41 mesh.

Figure 5 illustrates the entrance development length as a function of Reynolds number for the 101×41 mesh. Superimposed on the present results are the continuum development length equations presented by Atkinson *et al*. [12] and Chen [14]. Atkinson *et al*. suggested that the non-dimensionalised development length can be related to the Reynolds number via a simple linear relationship:

$$\frac{L}{D} = 0.59 + 0.056\,Re \tag{47}$$

whilst Chen [14] analysed development length data originally presented by Friedmann *et al.* [11] and proposed a more elaborate function of the form:

$$\frac{L}{D} = \frac{0.60}{0.035\,Re + 1} + 0.056\,Re \tag{48}$$

Figures 5 demonstrates that the present numerical results are in excellent agreement with the entrance lengths predicted by eqn. (48). In addition, it can be seen that Atkinson *et al.'s* solution tends to over-predict the development length at all but the lowest Reynolds numbers. This is confirmed in Figure 6 which shows an enlarged view of the development length variations for $0 \le Re \le 100$. Figure 6 also illustrates that the entrance length for a circular pipe tends towards an *L/D* ratio of approximately 0.60 as the Reynolds number approaches zero. Consequently, at low Reynolds numbers, the fully-developed velocity profile is established within about 0.6 pipe diameters of the entrance.

Figures 7 & 8 repeat the development length plots for the high resolution 201×101 mesh (Table 2). Comparison of the graphs for the two grid resolutions immediately confirms that mesh independent results are achieved using the lower resolution 101×41 grid. The results also demonstrate that rarefaction effects only have a marginal effect on the development length in circular pipes. It can therefore be concluded that Chen's development length formula (eqn. 48) derived for continuum flows is equally valid in the slip-flow regime.

6.2.2 *Flow between parallel plates*

Table 3 presents the corresponding hydrodynamic development lengths for the parallel plate geometry. A mesh resolution study was undertaken, and it was found that the 101×41 hydrodynamic grid once again yielded mesh independent results. It should be noted both the non-dimensionalised development length and the Reynolds number are based upon the *hydraulic diameter* of the duct, D_h.

The entrance lengths are illustrated in Figures 9 & 10 together with the development length equations presented by Atkinson *et al*. [12] and Chen [14]. In the case of flow between parallel plates, Atkinson *et al*. suggested that the non-dimensionalised development length can be related to the Reynolds number via the following linear relationship:

$$\frac{L}{D_h} = 0.3125 + 0.011\,Re \tag{49}$$

whereas Chen [14] suggested a more elaborate function of the form:

$$\frac{L}{D_h} = \frac{0.315}{0.0175\,Re + 1} + 0.011\,Re \tag{50}$$

Figures 9 & 10 indicate that the present continuum results ($Kn = 0$) are in good agreement with the hydrodynamic entrance lengths predicted by eqn. (50). It can also be seen that Atkinson *et al.'s* solution again tends to over-predict the development lengths except at very low Reynolds numbers. More importantly, the present results show that the Knudsen number has a significant effect on the length of the development region. Inspection of the L/D_h values in Table 3 reveals that at a Reynolds number of 400, the entrance length for a Knudsen number of 0.1 is 26% longer than the corresponding no-slip solution. Even at relatively low Reynolds numbers, the increase in hydrodynamic development length may still be important. For example, at a Reynolds number of 10, the entrance length for a Knudsen number of 0.1 is 13.6% longer than the continuum solution. It can therefore be concluded that the development length formulae proposed by Atkinson *et al.* [12] and Chen [14] for the parallel plate geometry cannot be applied to the slip-flow regime and consequently a new development length equation accounting for the variation in both the Reynolds number and Knudsen number must be evaluated.

To provide extra data for the subsequent least-squares analysis, additional development lengths were computed for Knudsen numbers of 0.025 and 0.075 (midway between the existing Knudsen numbers). Table 4 presents the complete set of entrance lengths employed in the analysis whilst Figure 11 provides a 3-dimensional representation of the data. A non-linear least-squares surface-fitting procedure employing the Levenberg-Marquardt method [38] was used to determine the equation of best fit; the analysis being performed using SigmaPlot, a commercial curve-fitting and graph plotting package. The effect of the Knudsen number was taken into account by multiplying Chen's original development length equation by correction factors of the form:

$$\left(\frac{1 + A\,Kn'}{1 + B\,Kn'}\right) \tag{51}$$

where A and B are constants and Kn' is defined as

$$Kn' = \frac{2 - \sigma}{\sigma}\,Kn \tag{52}$$

The Knudsen number variation shown in (51) was chosen because the analytical slip-flow equations developed in Appendix B have similar modification factors. Applying the Levenberg-Marquardt least-squares technique yields the following expression for the hydrodynamic development length:

$$\frac{L}{D_h} = \frac{0.320}{0.0272\,Re + 1}\left(\frac{1 + 13.51\,Kn'}{1 + 12.11\,Kn'}\right) + 0.011\,Re\left(\frac{1 + 14.75\,Kn'}{1 + 9.77\,Kn'}\right) \tag{53}$$

Estimation of the likely errors in each of the coefficients reveals that it is probably better to ignore the Knudsen number correction in the first term of eqn. (53) since the coefficients of 13.51 and 12.11 cannot be determined with any degree of accuracy. Consequently, a second least-squares analysis was conducted using a Knudsen number dependency on just the last term, giving:

$$\frac{L}{D_h} = \frac{0.332}{0.0271\,Re + 1} + 0.011\,Re\left(\frac{1 + 14.78\,Kn'}{1 + 9.78\,Kn'}\right) \tag{54}$$

Figure 12 illustrates the surface fit presented in eqn. (54). It can be seen that the proposed equation provides a good fit to the development length data over the range of Reynolds numbers considered. Moreover, the linearity of the Reynolds number dependency in the second term of eqn. (54) implies that the expression should provide a reliable estimate of hydrodynamic development lengths up to the transition to turbulence at approximately *Re*=2000. The proposed entrance length equation is therefore appropriate for the entire laminar slip-flow regime.

7 Conclusions

An investigation of low Reynolds number rarefied gas flows in circular pipes and parallel plates has been conducted using a specially adapted two-dimensional finite-volume Navier-Stokes solver. The hydrodynamic model is applicable to the *slip-flow regime* which is valid for Knudsen numbers between $0 < Kn \leq 0.1$. Within this range, rarefaction effects are important but the flow can still be modelled using the Navier-Stokes equations provided appropriate tangential slip-velocity boundary conditions are implemented along the walls of the flow domain.

The present study examines the effects of the Reynolds number and the Knudsen number on the hydrodynamic development length in circular pipes and parallel plates. Model validation has been accomplished by comparing numerical and analytical fully-developed velocity profiles across the ducts. In addition, hydrodynamic entrance lengths for the continuum (no-slip) regime are compared with data published in earlier studies. The results from the hydrodynamic model show that development lengths for the circular pipe are only marginally affected by rarefaction. However, it has been found that the Knudsen number can have a significant effect on the entrance development region for flows between parallel plates. At the upper limit of the slip-flow regime ($Kn \simeq 0.1$), entrance lengths for the parallel plate geometry can be up to 25% longer than the corresponding continuum solution. It is therefore important for designers of microfluidic devices to account for the possibility of increased development lengths in the gaseous slip-flow regime.

References

[1] Schlichting, H. *Boundary-Layer Theory*, 3rd English Ed., McGraw-Hill, 1968.

[2] Schlichting, H. Laminare Kanaleinlaufstromung, *Z.A.M.M.*, Vol. 14, pp. 368-373, 1934.

[3] Goldstein, S. *Modern Developments in Fluid Dynamics*, Vol. 1, Clarendon Press, Oxford, 1938: Atkinson & Goldstein, p. 304.

[4] Davies, R.T. Laminar incompressible flow past a semi-infinite flat plate, *J. Fluid Mech.*, Vol. 27, pp. 691-704, 1967.

[5] Van Dyke, M. Entry flow in a channel, *J. Fluid Mech.*, Vol. 44, pp. 813-823, 1970.

[6] Langhaar, H.L. Steady flow in the transition length of a straight tube, *Trans. of the ASME, J. Applied Mech.*, Vol. 9, A55-A58, 1942.

[7] Lundgren, T.S., Sparrow, E.M. & Starr, J.B. Pressure drop due to the entrance region in ducts of arbitrary cross-section, *Trans. of the ASME, J. Basic Engineering*, pp. 620-626, 1964.

[8] Han, L.S. Hydrodynamic entrance lengths for incompressible laminar flow in rectangular ducts, *Trans. of the ASME, J. Applied Mechanics*, Vol. 27, pp. 403-409, 1960.

[9] Bodoia, J.R. & Osterle, J.F. Finite-difference analysis of plane Poiseuille and Couette flow developments, *Applied Scientific Research*, Section A, Vol. 10, pp. 265-276, 1961.

[10] Wang, Y.L. & Longwell, P.A. Laminar flow in the inlet section of parallel plates, *A.I.Ch.E. Journal*, Vol. 10, No. 3, pp. 323-329, 1964.

[11] Friedmann, M., Gillis, J. & Liron, N. Laminar flow in a pipe at low and moderate Reynolds numbers, *Applied Scientific Research*, Vol. 19, pp. 426-438, 1968.

[12] Atkinson, B., Brocklebank, M.P., Card, C.C.H. & Smith, J.M. Low Reynolds number developing flows, *A.I.Ch.E. Journal*, Vol. 15, No. 4, pp. 548-553, 1969.

[13] Morihara, H. & Cheng, R.T.S. Numerical solution of the viscous flow in the entrance region of parallel plates, *J. Computational Physics*, Vol. 11, pp. 550-572, 1973.

[14] Chen, R.Y. Flow in the entrance region at low Reynolds numbers, *Trans. of the ASME, J. Fluids Engineering*, Vol. 95, pp. 153-158, 1973.

[15] Sparrow, E.M., Lundgren, T.S. & Lin, S.H. Slip flow in the entrance region of a parallel plate channel, *Proc. Heat Transfer and Fluid Mechanics Inst., Stanford University Press*, Paper no. 16, pp. 223-238, 1962.

[16] Ebert, W.A. & Sparrow, E.M. Slip flow in rectangular and annular ducts, *Trans. of the ASME, J. Basic Engineering*, Vol. 87, pp. 1018-1024, 1965.

[17] Sreekanth, A.K. Slip flow through long circular tubes, *Rarefied Gas Dynamics 6*, pp. 667-680, Academic Press, New York, 1968.

[18] Quarmby, A. A finite-difference analysis of developing slip flow, *Applied Scientific Research*, Vol. 19, pp. 18-33, 1968.

[19] Gampert, B. Inlet flow with slip, *Rarefied Gas Dynamics 10*, pp. 225-235, 1976.

[20] Gabriel, K., Jarvis, J. & Trimmer, W. (eds.) *Small Machines, Large Opportunities: a report on the emerging field of microdynamics*, National Science Foundation, AT&T Bell Laboratories, Murray Hill, New Jersey, USA, 1988.

[21] Gravesen, P., Branebjerg, J. & Jenson, O.S. Microfluidics – a review, *J. Micromechanics and Microengineering*, Vol. 3, pp. 168-182, 1993.

[22] Gad-el-Hak, M. The fluid mechanics of microdevices – The Freeman Scholar Lecture, *J. of Fluids Engineering*, Vol. 121, pp. 5-33, 1999.

[23] Beskok, A. & Karniadakis, G.E. Simulation of heat and momentum transfer in complex microgeometries, *J. Thermophysics and Heat Transfer*, Vol. 8, No. 4, 1994.

[24] Beskok, A., Karniadakis, G.E. & Trimmer, W. Rarefaction, compressibility and thermal creep effects in micro-flows, *Proc. of the ASME Dynamic Systems and Control Division*, pp. 877-892, ASME, 1995.

[25] Pfahler, J., Harley, J., Bau, H. & Zemel, J.N. Gas and liquid flow in small channels, DSC-Vol. 32, *Micromechanical Sensors, Actuators and Systems*, pp. 49-60, ASME, 1991.

[26] Harley, J.C., Huang, Y., Bau, H.H. & Zemel, J.N. Gas flow in microchannels, *J. Fluid Mech.*, Vol. 284, pp. 257-274, 1995.

[27] Arkilic, E.B. & Breuer, K.S. Gaseous flow in small channels, *AIAA Shear Flow Conference*, Paper no. AIAA 93-3270, Orlando, 1993.

[28] Arkilic, E.B., Breuer, K.S. & Schmidt, M.A. Gaseous flow in microchannels, FED-Vol. 197, *Application of Microfabrication to Fluid Mechanics*, pp. 57-66, ASME, 1994.

[29] Arkilic, E.B., Schmidt, M.A. & Breuer, K.S. Gaseous slip flow in long microchannels, *J. of Micro-Electro-Mechanical Systems*, Vol. 6, No. 2, pp. 167-178, 1997.

[30] Arkilic, E.B. *Measurement of the mass flow and tangential momentum accommodation coefficient in silicon micromachined channels*, Ph.D. Thesis, Massachusetts Institute of Technology, Cambridge, Massachusetts, 1997.

[31] Basset, A.B. *A Treatise on Hydrodynamics*, Cambridge University Press, 1888.

[32] Schaaf, S.A. & Chambre, P.L. *Flow of Rarefied Gases*, Princeton University Press, 1961.

[33] Thomas, L.B. & Lord, R.G. Comparative measurements of tangential momentum and thermal accommodations on polished and on roughened steel spheres, *Rarefied Gas Dynamics 8*, pp. 405-412, ed. K. Karamcheti, Academic Press, New York, 1974.

[34] Arkilic, E.B., Schmidt, M.A. & Breuer, K.S. TMAC measurement in silicon micromachined channels, *Rarefied Gas Dynamics 20*, Beijing University Press, 1997.

[35] Shah, R.K. & London, A.L. *Laminar Flow Forced Convection in Ducts*, Academic Press, New York, 1978.

[36] White, F.M. *Viscous Fluid Flow*, 2nd Edition, McGraw-Hill, 1991.
[37] Gu X.J. & Emerson, D.R. *THOR-2D: A two-dimensional computational fluid dynamics code*, Technical Report, Department of Computational Science and Engineering, CLRC Daresbury Laboratory, June 2000.
[38] Press, W.H., Teukolsky, S.A., Vetterling, W.T. & Flannery, B.P. *Numerical Recipes in Fortran: The Art of Scientific Computing*, 2nd Ed., Cambridge University Press, 1994.
[39] *CRC Handbook of Chemistry and Physics*, 80th Ed., CRC Press, 1999-2000.

Appendix A

Analysis of fully-developed laminar slip flow within a circular pipe

Consider an incompressible Newtonian fluid of density, ρ and viscosity, μ flowing through a long straight tube having a circular cross-section of radius, *R*. Let *x* denote the longitudinal distance along the axis of the pipe and let *r* denote the radial co-ordinate measured outwards from the centreline. Under fully-developed flow conditions, the velocity components in the radial- and tangential-directions are zero whilst the velocity component parallel to the longitudinal axis (denoted by *u*) is solely dependent upon *r*. In addition, the pressure is constant over a given cross-section of the pipe. Therefore, under fully-developed conditions, the flow can be described completely by the axial-direction Navier-Stokes equation, which in cylindrical co-ordinates reduces to

$$\mu\left(\frac{d^2u}{dr^2}+\frac{1}{r}\frac{du}{dr}\right)=\frac{dp}{dx} \tag{1}$$

where dp/dx is the pressure gradient in the longitudinal direction.

In order to account for non-continuum flow effects, eqn. (1) is solved in conjunction with the slip-velocity boundary condition proposed by Basset [31]:

$$\tau_t = \beta\, u_t \tag{2}$$

where u_t is the tangential slip-velocity at the wall, τ_t is the tangential shear stress on the wall and β is the slip coefficient. Schaaf & Chambre [32] show that the slip coefficient can be related to the mean free path of the molecules as follows:

$$\beta = \frac{\mu}{\left(\frac{2-\sigma}{\sigma}\right)\lambda} \tag{3}$$

where μ is the coefficient of viscosity, σ is the tangential momentum accommodation coefficient (TMAC) and λ is the mean free path of the gas. The tangential momentum accommodation coefficient is introduced into the equation to account for the reduction in the momentum of the molecules colliding with the wall. The value of the TMAC depends upon the particular solid and gas involved and also on the surface roughness of the wall. Equations (2) and (3) can be combined and rearranged to give

$$u_t = \frac{2-\sigma}{\sigma}\frac{\lambda}{\mu}\tau_t \tag{4}$$

At this stage, it is convenient to recast the mean free path in eqn. (4) in terms of a non-dimensionalised Knudsen number, *Kn*. For compatibility with the standard definition of Reynolds number for circular pipes, the characteristic length scale in the

present analysis is defined as the pipe diameter, D. Thus, eqn. (4) can be rewritten as

$$u_t = \frac{2-\sigma}{\sigma} \frac{Kn\, D}{\mu} \tau_t \tag{5}$$

where Kn is defined as the ratio of the mean free path of the molecules (λ) to the diameter of the pipe:

$$Kn = \frac{\lambda}{D} \tag{6}$$

The shear stress on the pipe wall ($r = R$) can be related to the velocity gradient as follows:

$$\tau_t = -\mu \left. \frac{du}{dr} \right|_{r=R} \tag{7}$$

The negative sign is introduced into the above expression to account for the fact that the velocity gradient, du/dr is negative. Substituting eqn. (7) into (5) then yields the tangential slip-velocity as

$$u_t = -\frac{2-\sigma}{\sigma} Kn\, D \left. \frac{du}{dr} \right|_{r=R} \tag{8}$$

The axial-direction Navier-Stokes equation (1) is a linear, second-order ordinary differential equation. It is assumed that the solution of (1) yields a velocity profile of the form:

$$u(r) = a\, r^2 + b\, r + c \tag{9}$$

where a, b and c are constants. Repeated differentiation of eqn. (9) gives

$$\left.\begin{aligned} u'(r) &= 2\, a\, r + b \\ u''(r) &= 2\, a \end{aligned}\right\} \tag{10}$$

and substituting the derivatives shown in (10) into the original differential equation yields

$$2\, a + \frac{1}{r}\left(2\, a\, r + b\right) = \frac{1}{\mu} \frac{dp}{dx} \tag{11}$$

which can be rearranged to give

$$\left(4a - \frac{1}{\mu}\frac{dp}{dx}\right) r + b = 0 \tag{12}$$

Inspection of eqn. (12) thus reveals

$$a = \frac{1}{4\mu}\frac{dp}{dx} \qquad \text{and} \qquad b = 0 \tag{13}$$

The zero-order coefficient, *c*, is determined using the slip-velocity constraint shown in eqn. (8). First, the velocity gradient at the wall is found by substituting $b = 0$ into eqn. (10):

$$\left.\frac{du}{dr}\right|_{r=R} = \frac{R}{2\mu}\frac{dp}{dx} \tag{14}$$

Hence, the tangential slip-velocity at the wall is given by

$$u_t = -\frac{2-\sigma}{\sigma} Kn\, D\, \frac{R}{2\mu}\frac{dp}{dx} \tag{15}$$

or

$$u_t = -\frac{2-\sigma}{\sigma} Kn\, R^2\, \frac{1}{\mu}\frac{dp}{dx} \tag{16}$$

The tangential slip-velocity is then substituted into the velocity profile proposed in eqn. (9):

$$\frac{1}{4\mu}\frac{dp}{dx} R^2 + c = -\frac{2-\sigma}{\sigma} Kn\, R^2\, \frac{1}{\mu}\frac{dp}{dx} \tag{17}$$

which can be rearranged to give

$$c = -\frac{1}{4\mu}\frac{dp}{dx}\left(R^2 + 4\frac{2-\sigma}{\sigma} Kn\, R^2\right) \tag{18}$$

Thus the velocity profile across the pipe is given by

$$u(r) = \frac{1}{4\mu}\frac{dp}{dx} r^2 - \frac{1}{4\mu}\frac{dp}{dx}\left(R^2 + 4\frac{2-\sigma}{\sigma} Kn\, R^2\right) \tag{19}$$

which can be rewritten as

$$u(r) = -\frac{1}{4\mu}\frac{dp}{dx}\left(R^2 - r^2 + 4\frac{2-\sigma}{\sigma} Kn\, R^2\right) \tag{20}$$

It can therefore be seen that the velocity profile over the cross-section takes the form of a paraboloid of revolution. As an aside, in the limit of $Kn \to 0$ (continuum flow)

we obtain the no-slip (NS) solution given by Hagen-Poiseuille theory for flow through a circular pipe (see Schlichting [1]):

$$u_{\mathrm{NS}}(r) = -\frac{1}{4\mu}\frac{dp}{dx}\left(R^2 - r^2\right) \tag{21}$$

The maximum velocity in the pipe occurs at the centreline ($r = 0$):

$$u_{\max} = -\frac{R^2}{4\mu}\frac{dp}{dx}\left(1 + 4\frac{2-\sigma}{\sigma}Kn\right) \tag{22}$$

In addition, let $\bar{u}$ denote the mean or average velocity in the pipe, defined by

$$\bar{u} = \frac{1}{\pi R^2}\int_0^R u(r)\, 2\pi r\, dr \tag{23}$$

Substituting eqn. (20) into (23) yields

$$\bar{u} = \frac{1}{\pi R^2}\int_0^R -\frac{1}{4\mu}\frac{dp}{dx}\left(R^2 - r^2 + 4\frac{2-\sigma}{\sigma}Kn\, R^2\right) 2\pi r\, dr \tag{24}$$

which can be simplified to

$$\bar{u} = -\frac{1}{4\mu}\frac{dp}{dx}\frac{2}{R^2}\int_0^R \left(R^2 r - r^3 + 4\frac{2-\sigma}{\sigma}Kn\, R^2\, r\right) dr \tag{25}$$

Integrating and rearranging finally leads to the mean velocity:

$$\bar{u} = -\frac{R^2}{4\mu}\frac{dp}{dx}\frac{1}{2}\left(1 + 8\frac{2-\sigma}{\sigma}Kn\right) \tag{26}$$

Hence, the ratio of the maximum velocity at the centreline of the pipe to the mean velocity is given by

$$\frac{u_{\max}}{\bar{u}} = \frac{\left(1 + 4\frac{2-\sigma}{\sigma}Kn\right)}{\frac{1}{2}\left(1 + 8\frac{2-\sigma}{\sigma}Kn\right)} \tag{27}$$

and therefore the maximum velocity in the pipe is found to be

$$u_{\max} = 2\bar{u}\,\frac{\left(1+4\dfrac{2-\sigma}{\sigma}Kn\right)}{\left(1+8\dfrac{2-\sigma}{\sigma}Kn\right)} \tag{28}$$

Allowing $Kn \to 0$ yields the familiar no-slip (NS) solution given by Hagen-Poiseuille pipe theory:

$$u_{\max(\mathrm{NS})} = 2\bar{u} \tag{29}$$

Similarly, eqns. (20) and (26) can be combined to give the velocity distribution across the pipe in terms of the mean velocity:

$$\frac{u(r)}{\bar{u}} = \frac{\left(1-\dfrac{r^2}{R^2}+4\dfrac{2-\sigma}{\sigma}Kn\right)}{\dfrac{1}{2}\left(1+8\dfrac{2-\sigma}{\sigma}Kn\right)} \tag{30}$$

or

$$u(r) = 2\bar{u}\,\frac{\left(1-\dfrac{r^2}{R^2}+4\dfrac{2-\sigma}{\sigma}Kn\right)}{\left(1+8\dfrac{2-\sigma}{\sigma}Kn\right)} \tag{31}$$

The tangential slip-velocity at the wall, u_t, can then be found by prescribing $r = R$ in eqn. (31):

$$u_t = \bar{u}\,\frac{8\dfrac{2-\sigma}{\sigma}Kn}{\left(1+8\dfrac{2-\sigma}{\sigma}Kn\right)} \tag{32}$$

In addition, the volume rate of flow in the circular pipe is given by

$$Q = \pi R^2 \bar{u} = -\frac{\pi}{8}\frac{R^4}{\mu}\frac{dp}{dx}\left(1+8\frac{2-\sigma}{\sigma}Kn\right) \tag{33}$$

Hence, in the limit of $Kn \to 0$ we obtain the no-slip (NS) solution for the volume rate of flow:

$$Q_{\mathrm{NS}} = \pi R^2 \bar{u}_{\mathrm{NS}} = -\frac{\pi}{8}\frac{R^4}{\mu}\frac{dp}{dx} \tag{34}$$

Dividing eqn. (33) by (34) yields

$$\frac{Q}{Q_{\mathrm{NS}}} = 1 + 8\frac{2-\sigma}{\sigma} Kn \tag{35}$$

The above equation indicates that even at relatively low Knudsen numbers, the slip-velocity boundary condition substantially increases the volume rate of flow through the pipe.

Finally, substituting eqn. (32) for the tangential slip-velocity at the wall into eqn. (2) yields the shear stress on the wall:

$$\tau_t = \frac{\mu\,\bar{u}}{\left(\frac{2-\sigma}{\sigma}\right)\lambda} \; \frac{8\frac{2-\sigma}{\sigma} Kn}{\left(1 + 8\frac{2-\sigma}{\sigma} Kn\right)} \tag{36}$$

which can be rewritten as

$$\tau_t = \frac{8\,\mu\,\bar{u}}{D\left(1 + 8\frac{2-\sigma}{\sigma} Kn\right)} \tag{37}$$

Furthermore, by defining the Reynolds number, *Re*, in the pipe as

$$Re = \frac{\rho\,\bar{u}\,D}{\mu} \tag{38}$$

eqn. (37) can be expressed as

$$\tau_t = \frac{8\,\mu^2\,Re}{\rho\,D^2\left(1 + 8\frac{2-\sigma}{\sigma} Kn\right)} \tag{39}$$

The no-slip solution is found by considering $Kn \to 0$. This yields the shear stress on the wall as

$$\tau_{t\,(\mathrm{NS})} = \frac{8\,\mu^2\,Re}{\rho\,D^2} \tag{40}$$

Appendix B

Analysis of fully-developed laminar slip flow between parallel plates

The analysis of laminar slip flow between parallel plates essentially follows a similar procedure to that detailed in Appendix A for circular pipes. The geometry is important as it forms the limiting flow condition for large aspect ratio rectangular ducts commonly encountered in microfluidic devices.

Consider an incompressible Newtonian fluid of density, ρ and viscosity, μ flowing between two parallel plates separated by a distance, *H*, as illustrated in the diagram below:

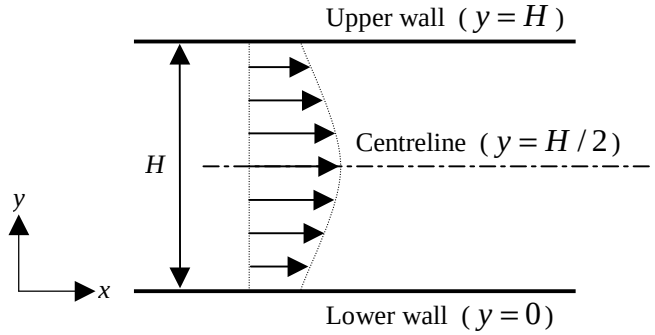

Figure B1: Slip flow between parallel plates

Let *x* denote the longitudinal distance along the duct and let *y* denote the normal distance measured upwards from the lower wall. Under fully-developed flow conditions, the velocity component in the *y*-direction vanishes and the velocity component in the *x*-direction (denoted by *u*) is solely dependent upon *y*. In addition, the pressure is constant over a given cross-section of the duct. Therefore, under fully-developed conditions, the flow can be described completely by the *x*-direction Navier-Stokes equation which reduces to

$$\mu \frac{d^2u}{dy^2} = \frac{dp}{dx} \tag{1}$$

where dp/dx is the pressure gradient in the longitudinal direction.

In order to account for non-continuum flow effects, eqn. (1) is solved in conjunction with the slip-velocity boundary condition proposed by Basset [31]:

$$\tau_t = \beta\, u_t \tag{2}$$

where u_t is the tangential slip-velocity at the wall, τ_t is the tangential shear stress on the wall and β is the slip coefficient. Schaaf & Chambre [32] show that the slip coefficient can be related to the mean free path of the molecules as follows:

$$\beta = \frac{\mu}{\left(\frac{2-\sigma}{\sigma}\right)\lambda} \tag{3}$$

where μ is the coefficient of viscosity, σ is the tangential momentum accommodation coefficient (TMAC) and λ is the mean free path of the molecules. Equations (2) and (3) can be combined and rearranged to give

$$u_t = \frac{2-\sigma}{\sigma}\frac{\lambda}{\mu}\tau_t \tag{4}$$

At this stage, it is convenient to recast the mean free path in eqn. (4) in terms of the non-dimensionalised Knudsen number, *Kn*. Analyses of non-circular ducts generally rely upon the concept of the *hydraulic diameter*, D_h, as detailed by Schlichting [1], Shah & London [35] or White [36]:

$$D_h = \frac{4\times\text{area}}{\text{wetted perimeter}} = \frac{4A}{P} \tag{5}$$

Thus it is customary to define the Reynolds number in non-circular ducts in terms of the hydraulic diameter, i.e.

$$Re = \frac{\rho\,\bar{u}\,D_h}{\mu} \tag{6}$$

where $\bar{u}$ is the mean or average velocity in the duct. In the case of flow between parallel plates, it can readily be shown that the hydraulic diameter is twice the separation of the plates:

$$D_h = 2H \tag{7}$$

and therefore the Reynolds number in the present analysis is defined as

$$Re = \frac{\rho\,\bar{u}\,2H}{\mu} \tag{8}$$

For compatibility with the above definition of Reynolds number, the hydraulic diameter should also be employed as the characteristic length scale when determining the Knudsen number, *Kn*. Consequently, the tangential slip-velocity equation (4) can be rewritten as

$$u_t = \frac{2-\sigma}{\sigma}\frac{Kn\,2H}{\mu}\tau_t \tag{9}$$

where *Kn* is defined as the ratio of the mean free path of the molecules (λ) to the

hydraulic diameter:

$$Kn = \frac{\lambda}{D_h} = \frac{\lambda}{2H} \tag{10}$$

The shear stress on the lower wall of the duct ($y = 0$) can be related to the velocity gradient as follows:

$$\tau_t = \mu \left. \frac{du}{dy} \right|_{y=0} \tag{11}$$

As an aside, the shear stress on the upper wall of the duct ($y = H$) is evaluated using a very similar equation with the exception of a negative sign to account for the change in direction of the velocity gradient at the upper wall. Substituting eqn. (11) into (9) then yields the tangential slip-velocity as

$$u_t = \frac{2-\sigma}{\sigma} Kn\, 2H \left. \frac{du}{dy} \right|_{y=0} \tag{12}$$

The *x*-direction Navier-Stokes equation (1) is a linear, second-order ordinary differential equation. It is assumed that the solution of (1) yields a velocity profile of the form:

$$u(y) = a\, y^2 + b\, y + c \tag{13}$$

where *a*, *b* and *c* are constants. Repeated differentiation of eqn. (13) yields

$$\left.\begin{aligned} u'(y) &= 2\, a\, y + b \\ u''(y) &= 2\, a \end{aligned}\right\} \tag{14}$$

and substituting the second derivative, $u''(y)$ into the original differential equation gives

$$a = \frac{1}{2\mu} \frac{dp}{dx} \tag{15}$$

The first-order coefficient, *b*, is determined by employing the fact that the velocity profile between the plates is symmetrical. Consequently,

$$u'(y) = 0 \quad \text{at} \quad y = \frac{H}{2} \tag{16}$$

giving

$$b = -a\, H = -\frac{H}{2\mu} \frac{dp}{dx} \tag{17}$$

Finally, the zero-order coefficient, c, is evaluated using the slip-velocity constraint shown in eqn. (12). The velocity gradient at the lower wall is found by substituting $y = 0$ into eqn. (14) giving

$$\left.\frac{du}{dy}\right|_{y=0} = -\frac{H}{2\mu}\frac{dp}{dx} \tag{18}$$

and therefore the tangential slip-velocity is given by

$$u_t = -\frac{2-\sigma}{\sigma} Kn\, 2H\, \frac{H}{2\mu}\frac{dp}{dx} \tag{19}$$

The tangential slip-velocity is then substituted back into the velocity profile shown in eqn. (13) to give

$$c = -\frac{2-\sigma}{\sigma} Kn\, H^2\, \frac{1}{\mu}\frac{dp}{dx} \tag{20}$$

Thus the velocity profile across the duct takes the form:

$$u(y) = \frac{1}{2\mu}\frac{dp}{dx} y^2 - \frac{H}{2\mu}\frac{dp}{dx} y - \frac{2-\sigma}{\sigma} Kn\, H^2\, \frac{1}{\mu}\frac{dp}{dx} \tag{21}$$

which can be rewritten as

$$u(y) = -\frac{H^2}{2\mu}\frac{dp}{dx}\left(\frac{y}{H} - \frac{y^2}{H^2} + 2\frac{2-\sigma}{\sigma} Kn\right) \tag{22}$$

As an aside, in the limit of $Kn \to 0$ (continuum flow) we obtain the familiar no-slip (NS) formula for parallel flow through a straight channel (see Schlichting [1]):

$$u_{\mathrm{NS}}(y) = -\frac{H^2}{2\mu}\frac{dp}{dx}\left(\frac{y}{H} - \frac{y^2}{H^2}\right) \tag{23}$$

The maximum velocity occurs at the centreline of the duct ($y = H/2$):

$$u_{\max} = -\frac{H^2}{2\mu}\frac{dp}{dx}\left(\frac{1}{2} - \frac{1}{4} + 2\frac{2-\sigma}{\sigma} Kn\right) \tag{24}$$

or

$$u_{\max} = -\frac{H^2}{2\mu}\frac{dp}{dx}\frac{1}{4}\left(1 + 8\frac{2-\sigma}{\sigma} Kn\right) \tag{25}$$

In addition, let $\bar{u}$ denote the mean or average velocity in the duct, defined by

$$\bar{u} = \frac{1}{H}\int_0^H u(y)\,dy \tag{26}$$

Substituting eqn. (22) into (26) yields

$$\bar{u} = \frac{1}{H}\int_0^H -\frac{H^2}{2\mu}\frac{dp}{dx}\left(\frac{y}{H} - \frac{y^2}{H^2} + 2\frac{2-\sigma}{\sigma}Kn\right)dy \tag{27}$$

Integrating and rearranging leads to the mean velocity:

$$\bar{u} = -\frac{H^2}{2\mu}\frac{dp}{dx}\frac{1}{6}\left(1+12\frac{2-\sigma}{\sigma}Kn\right) \tag{28}$$

Hence, the ratio of the maximum velocity to the mean velocity is given by

$$\frac{u_{\max}}{\bar{u}} = \frac{\frac{1}{4}\left(1+8\frac{2-\sigma}{\sigma}Kn\right)}{\frac{1}{6}\left(1+12\frac{2-\sigma}{\sigma}Kn\right)} \tag{29}$$

and therefore the maximum velocity in the duct equals

$$u_{\max} = \frac{3}{2}\bar{u}\,\frac{\left(1+8\frac{2-\sigma}{\sigma}Kn\right)}{\left(1+12\frac{2-\sigma}{\sigma}Kn\right)} \tag{30}$$

Allowing $Kn \to 0$ yields the familiar no-slip solution:

$$u_{\max(\mathrm{NS})} = \frac{3}{2}\bar{u} \tag{31}$$

Similarly, eqns. (22) and (28) can be combined to give the velocity distribution across the duct in terms of the mean velocity:

$$\frac{u(y)}{\bar{u}} = \frac{\left(\frac{y}{H} - \frac{y^2}{H^2} + 2\frac{2-\sigma}{\sigma} Kn \right)}{\frac{1}{6}\left(1+12\frac{2-\sigma}{\sigma} Kn \right)} \tag{32}$$

or

$$u(y) = 6\bar{u} \frac{\left(\frac{y}{H} - \frac{y^2}{H^2} + 2\frac{2-\sigma}{\sigma} Kn \right)}{\left(1+12\frac{2-\sigma}{\sigma} Kn \right)} \tag{33}$$

The tangential slip-velocity at the wall, u_t, can then be found by prescribing $y = 0$ in eqn. (33):

$$u_t = \bar{u} \frac{12\frac{2-\sigma}{\sigma} Kn}{\left(1+12\frac{2-\sigma}{\sigma} Kn \right)} \tag{34}$$

In addition, the volume rate of flow per unit width of duct, *q*, is given by

$$q = H\bar{u} = -\frac{H^3}{2\mu}\frac{dp}{dx}\frac{1}{6}\left(1+12\frac{2-\sigma}{\sigma} Kn \right) \tag{35}$$

Hence, in the limit of $Kn \to 0$ we obtain the no-slip solution for the volume rate of flow:

$$q_{NS} = H\bar{u}_{NS} = -\frac{H^3}{2\mu}\frac{dp}{dx}\frac{1}{6} \tag{36}$$

Dividing eqn. (35) by (36) yields

$$\frac{q}{q_{NS}} = 1+12\frac{2-\sigma}{\sigma} Kn \tag{37}$$

The above equation indicates that even at relatively low Knudsen numbers, the slip-velocity boundary condition substantially increases the volume rate of flow through the duct.

Finally, substituting eqn. (34) for the tangential slip-velocity at the wall into eqn. (2) yields the shear stress on the wall:

$$\tau_t = \frac{\mu \bar{u}}{\left(\frac{2-\sigma}{\sigma}\right)\lambda} \frac{12\frac{2-\sigma}{\sigma}Kn}{\left(1+12\frac{2-\sigma}{\sigma}Kn\right)} \tag{38}$$

which can be rewritten as

$$\tau_t = \frac{12\,\mu\,\bar{u}}{2H\left(1+12\frac{2-\sigma}{\sigma}Kn\right)} \tag{39}$$

Furthermore, since the Reynolds number in the duct is defined as

$$Re = \frac{\rho \bar{u}\, 2H}{\mu} \tag{40}$$

eqn. (39) can be expressed as

$$\tau_t = \frac{3\mu^2\, Re}{\rho H^2\left(1+12\frac{2-\sigma}{\sigma}Kn\right)} \tag{41}$$

The no-slip solution is found by considering $Kn \to 0$. This yields the shear stress on the wall as

$$\tau_{t\,(\mathrm{NS})} = \frac{3\mu^2\, Re}{\rho H^2} \tag{42}$$

Appendix C

Determination of the mean free path of a gas

For an ideal gas modelled as rigid spheres of diameter, σ, the mean distance travelled by a molecule between successive collisions or *mean free path*, λ, is given by [39]:

$$\lambda = \frac{k\,T}{\sqrt{2}\,\pi\,p\,\sigma^2} \tag{1}$$

where,

k = Boltzmann's constant $= 1.380662\times10^{-23}$ J / K,

T = temperature (K),

p = pressure (N/m^2) and

σ = collision diameter of the molecules (m).

At standard ambient temperature and pressure (SATP), defined as T = 298.15 K and $p = 10^5$ N/m^2, eqn. (1) becomes:

$$\lambda = \frac{9.265\times10^{-27}}{\sigma^2} \tag{2}$$

For air, the average collision diameter of the molecules is 3.66×10^{-10} m giving a mean free path of 6.92×10^{-8} m (or 69.2 nm).

The table below details the collision diameters of other common gases.

Gas	σ (m)
Air	3.66×10^{-10}
Ar	3.58×10^{-10}
CO_2	4.53×10^{-10}
H_2	2.71×10^{-10}
He	2.15×10^{-10}
Kr	4.08×10^{-10}
N_2	3.70×10^{-10}
NH_3	4.32×10^{-10}
Ne	2.54×10^{-10}
O_2	3.55×10^{-10}
Xe	4.78×10^{-10}

Table C1: Collision diameters of common gases [39]

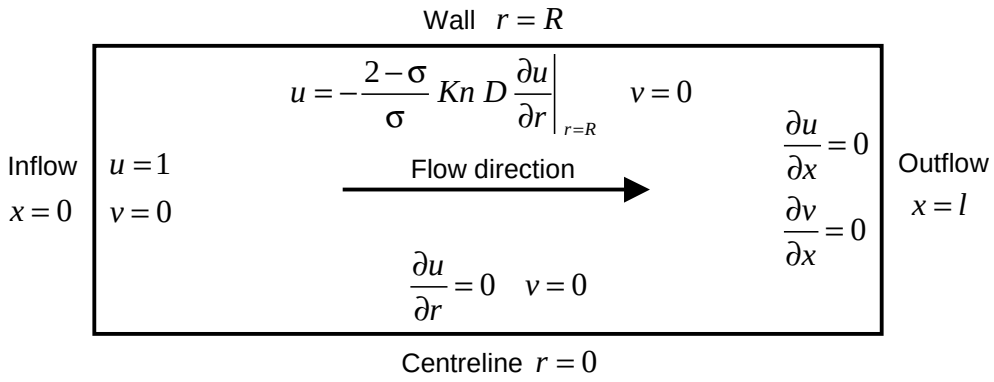

Figure 1: Schematic layout of boundary conditions for circular pipe geometry

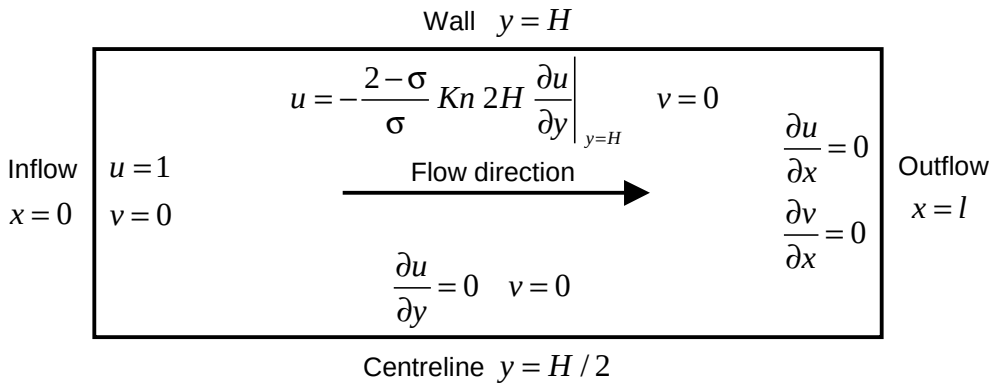

Figure 2: Schematic layout of boundary conditions for parallel plate geometry

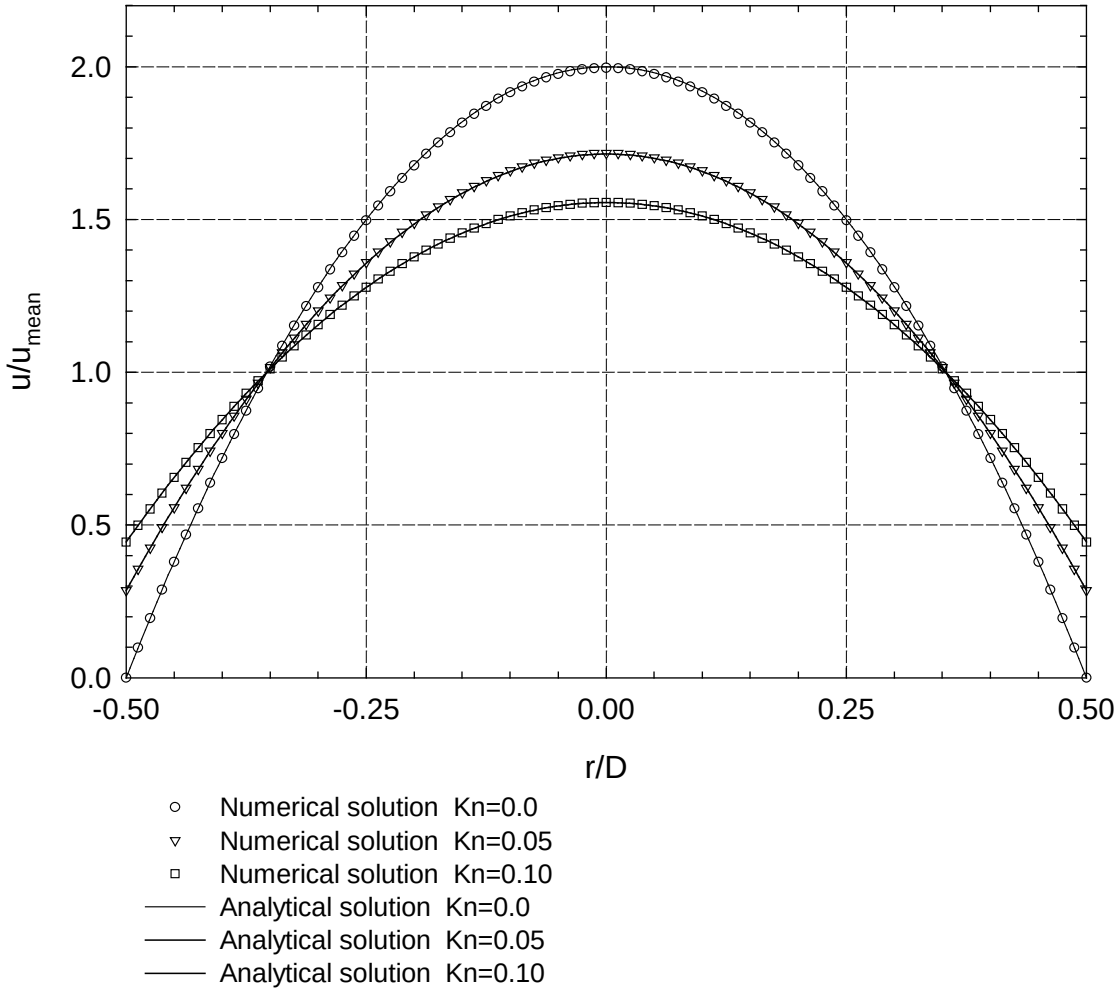

Figure 3: Fully-developed velocity profiles for a circular pipe
(101x41 mesh)

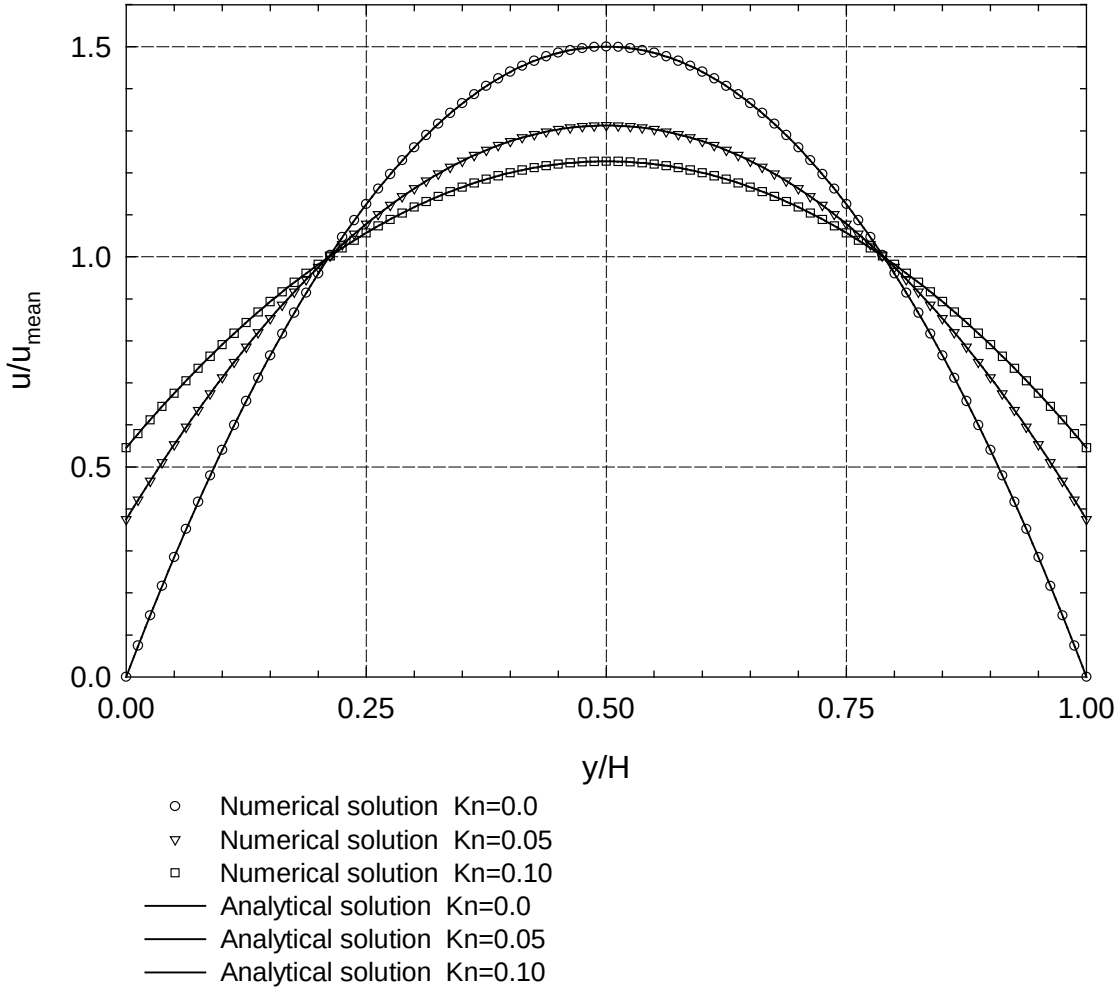

Figure 4: Fully-developed velocity profiles for flow between parallel plates (101x41 mesh)

Re	Kn=0.0	Kn=0.05	Kn=0.10
	L/D	L/D	L/D
1	0.6238	0.6618	0.6753
5	0.7126	0.7564	0.7746
10	0.8799	0.9254	0.9454
20	1.3483	1.3835	1.3953
40	2.4331	2.4480	2.4463
60	3.5483	3.5500	3.5394
80	4.6780	4.6670	4.6470
100	5.8035	5.7816	5.7564
150	8.6236	8.5707	8.5330
200	11.4460	11.3652	11.3158
250	14.2749	14.1606	14.0974
300	17.0736	16.9215	16.8450
350	19.7880	19.6097	19.5247
400	22.3624	22.1373	22.0322

Table 1: Non-dimensionalised development lengths for a circular pipe (101×41 mesh)

Re	Kn=0.0	Kn=0.05	Kn=0.10
	L/D	L/D	L/D
1	0.6210	0.6579	0.6732
5	0.7094	0.7528	0.7718
10	0.8766	0.9221	0.9418
20	1.3462	1.3791	1.3924
40	2.4303	2.4444	2.4428
60	3.5462	3.5473	3.5362
80	4.6689	4.6590	4.6400
100	5.7931	5.7732	5.7472
150	8.6017	8.5612	8.5222
200	11.4061	11.3497	11.2999
250	14.2025	14.1337	14.0728
300	16.9717	16.8925	16.8229
350	19.6703	19.5786	19.4996
400	22.2270	22.1284	22.0392

Table 2: Non-dimensionalised development lengths for a circular pipe (201×101 mesh)

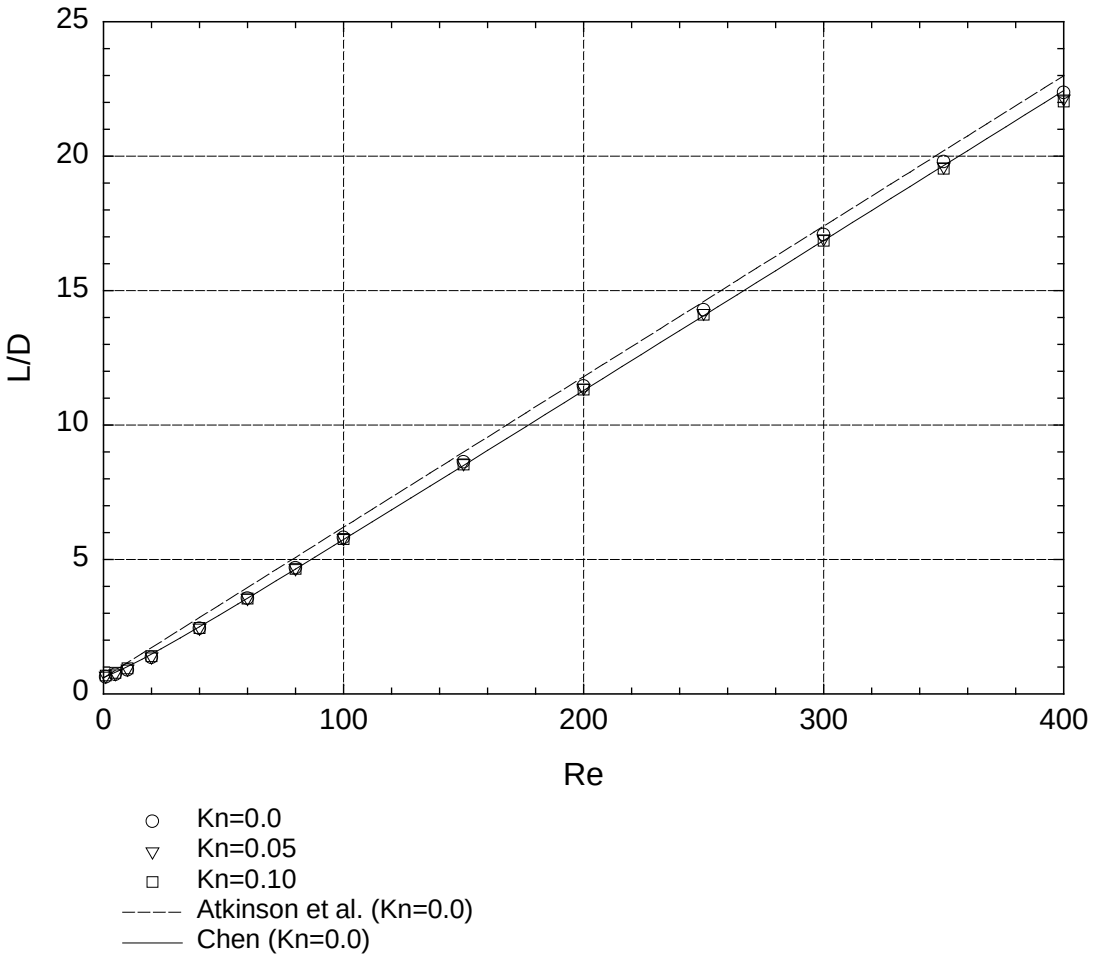

Figure 5: Non-dimensionalised development lengths for a circular pipe (101×41 mesh)

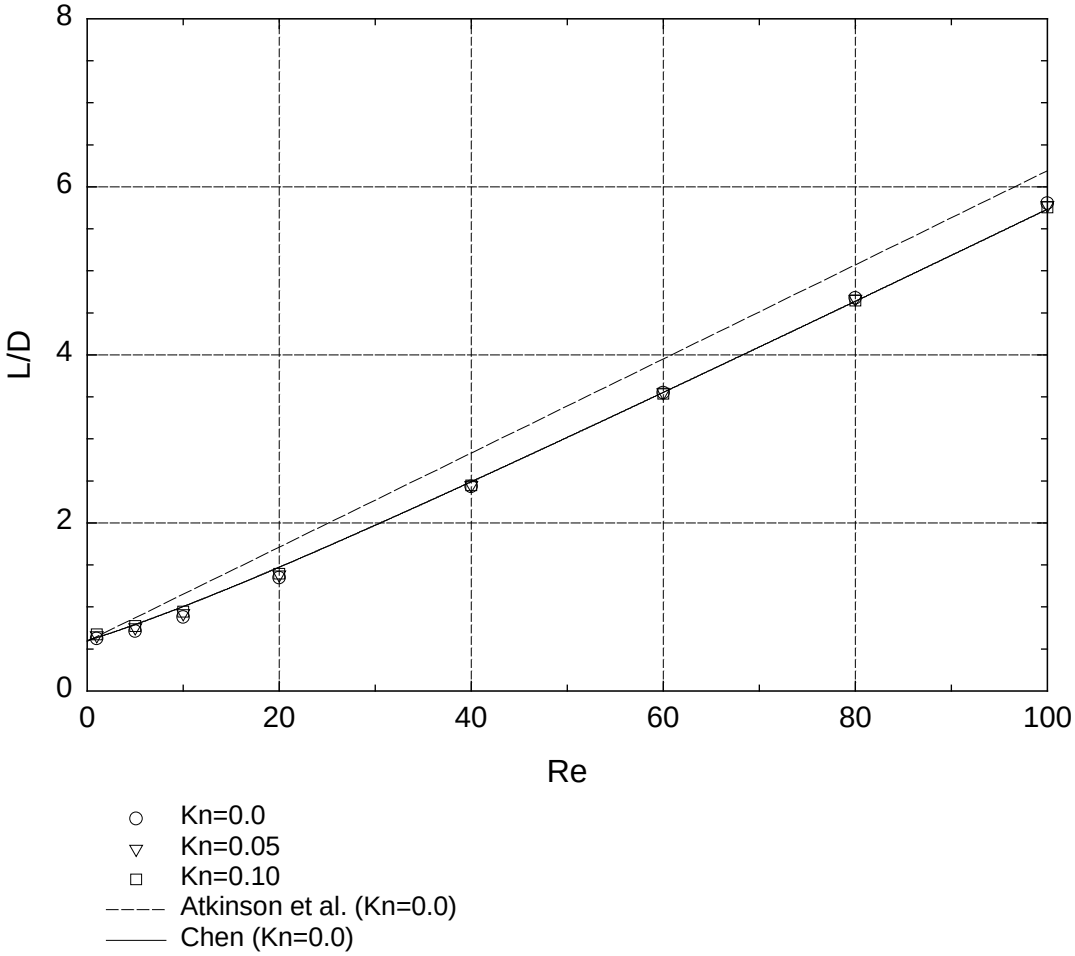

Figure 6: Detail of non-dimensionalised development lengths for a circular pipe (101×41 mesh)

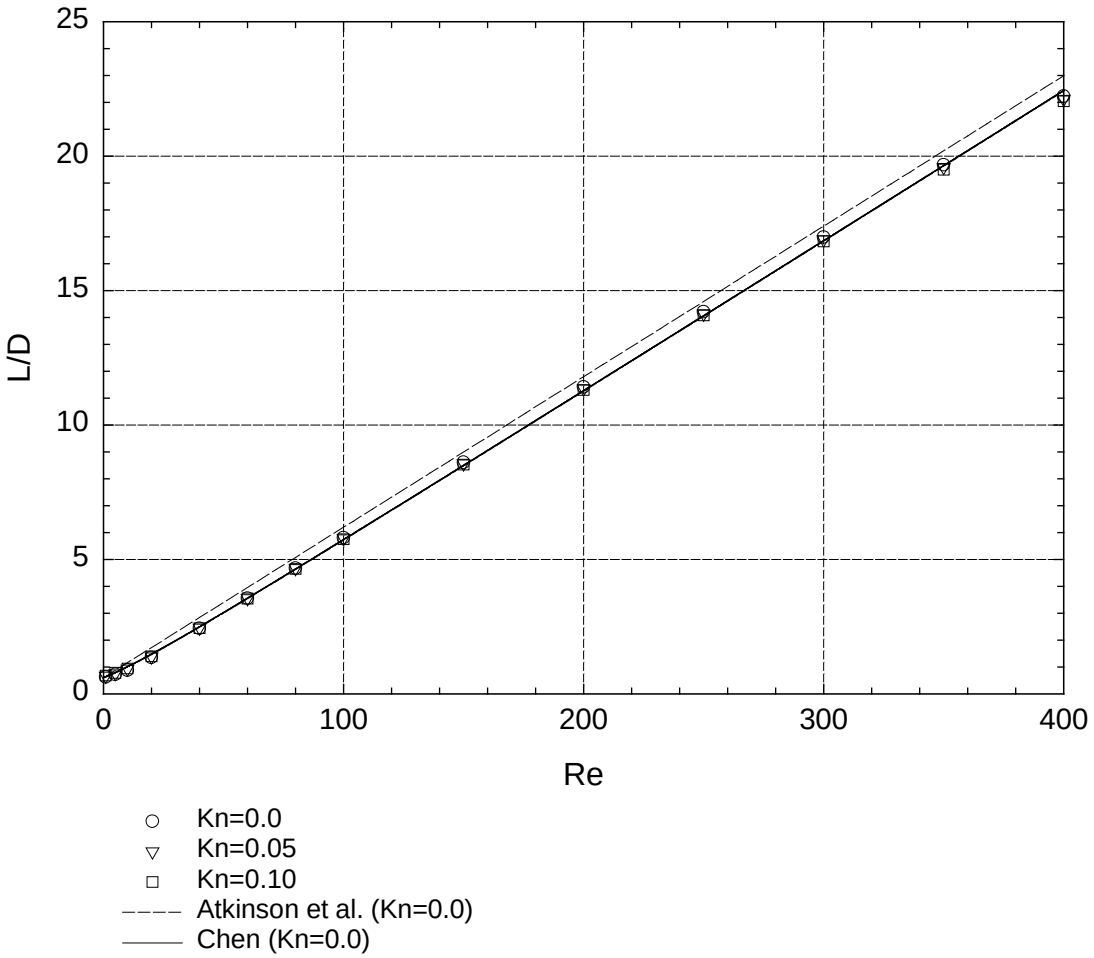

Figure 7: Non-dimensionalised development lengths for a circular pipe (201×101 mesh)

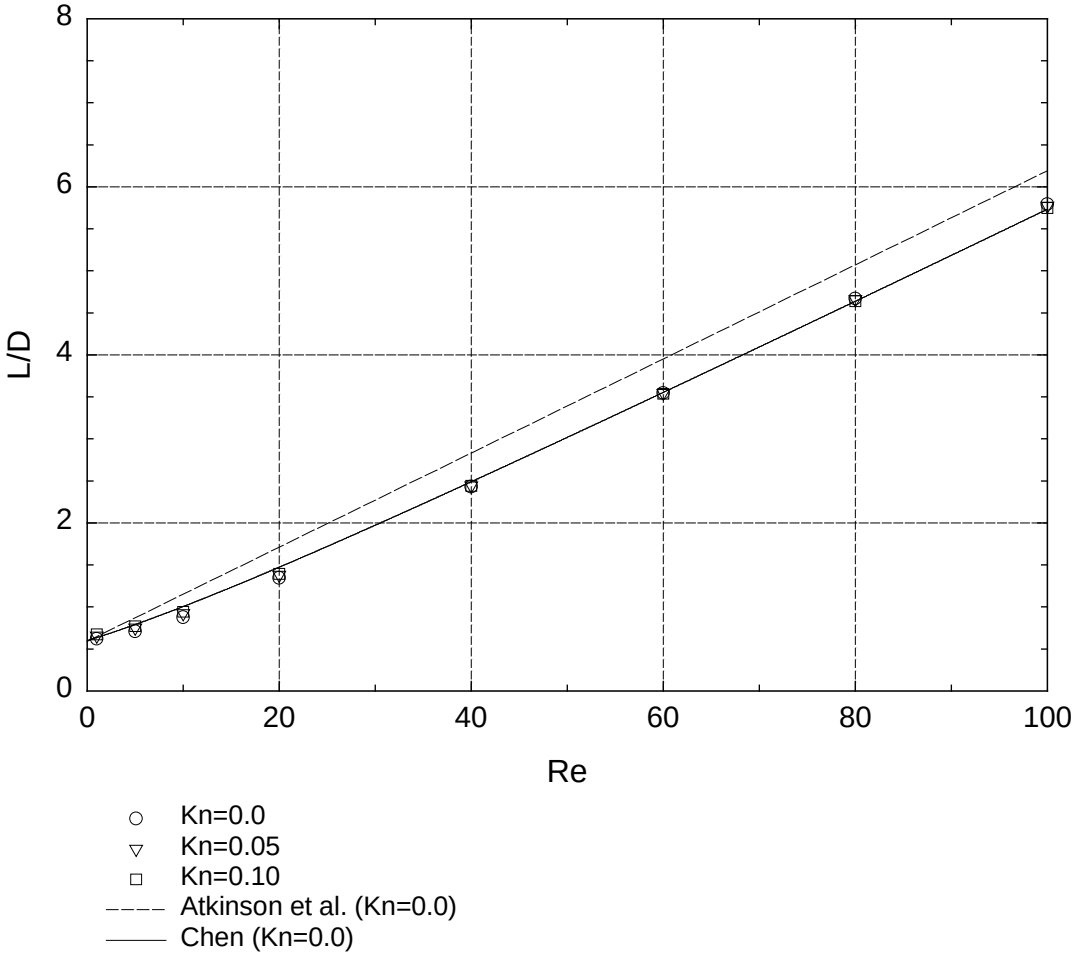

Figure 8: Detail of non-dimensionalised development lengths for a circular pipe (201×101 mesh)

Re	Kn=0.0	Kn=0.05	Kn=0.10
	L/D_h	L/D_h	L/D_h
1	0.3238	0.3473	0.3488
5	0.3360	0.3646	0.3703
10	0.3544	0.3915	0.4027
20	0.4092	0.4636	0.4849
40	0.5706	0.6583	0.6975
60	0.7769	0.8892	0.9436
80	0.9945	1.1316	1.2016
100	1.2141	1.3795	1.4640
150	1.7589	2.0057	2.1296
200	2.2966	2.6340	2.7994
250	2.8240	3.2633	3.4711
300	3.3425	3.8916	4.1447
350	3.8533	4.5224	4.8151
400	4.3555	5.1509	5.4898

Table 3: Non-dimensionalised development lengths for flow between parallel plates (101×41 mesh)

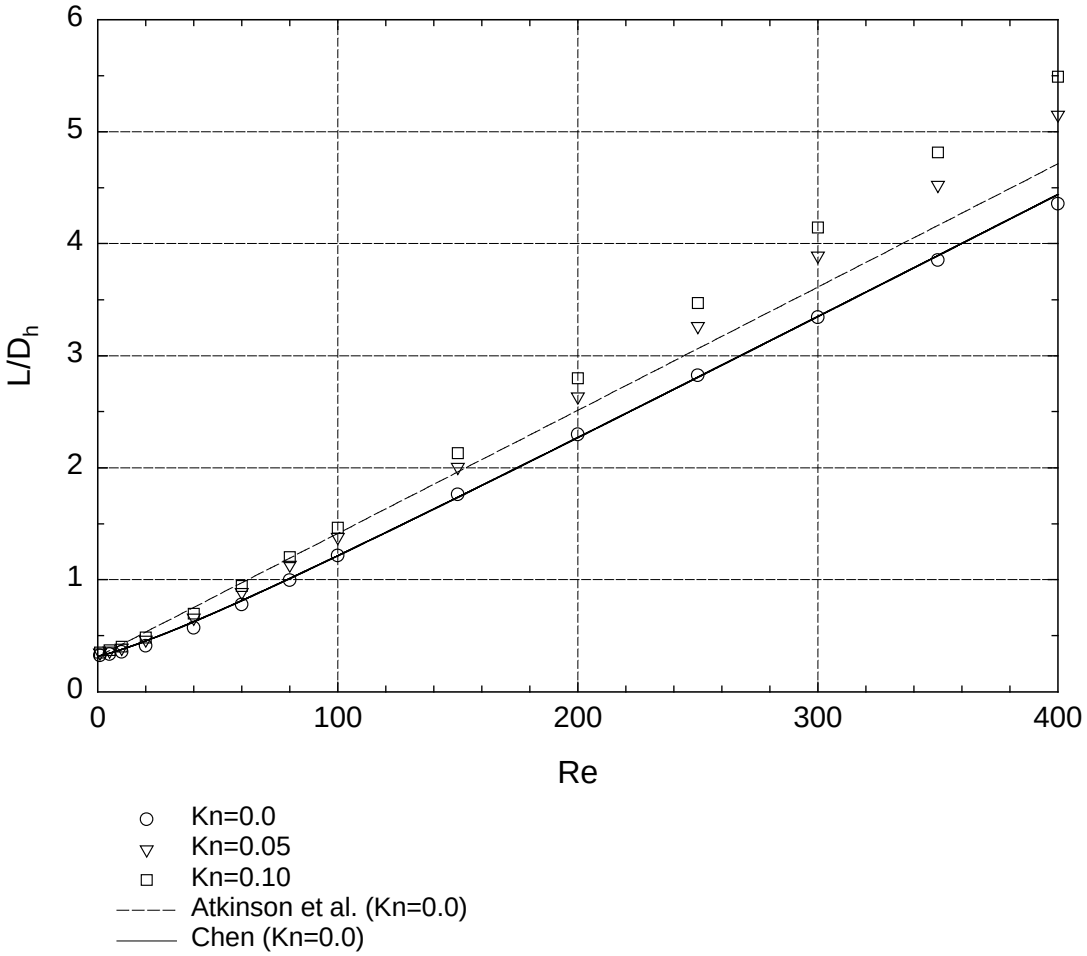

Figure 9: Non-dimensionalised development lengths for flow between parallel plates (101×41 mesh)

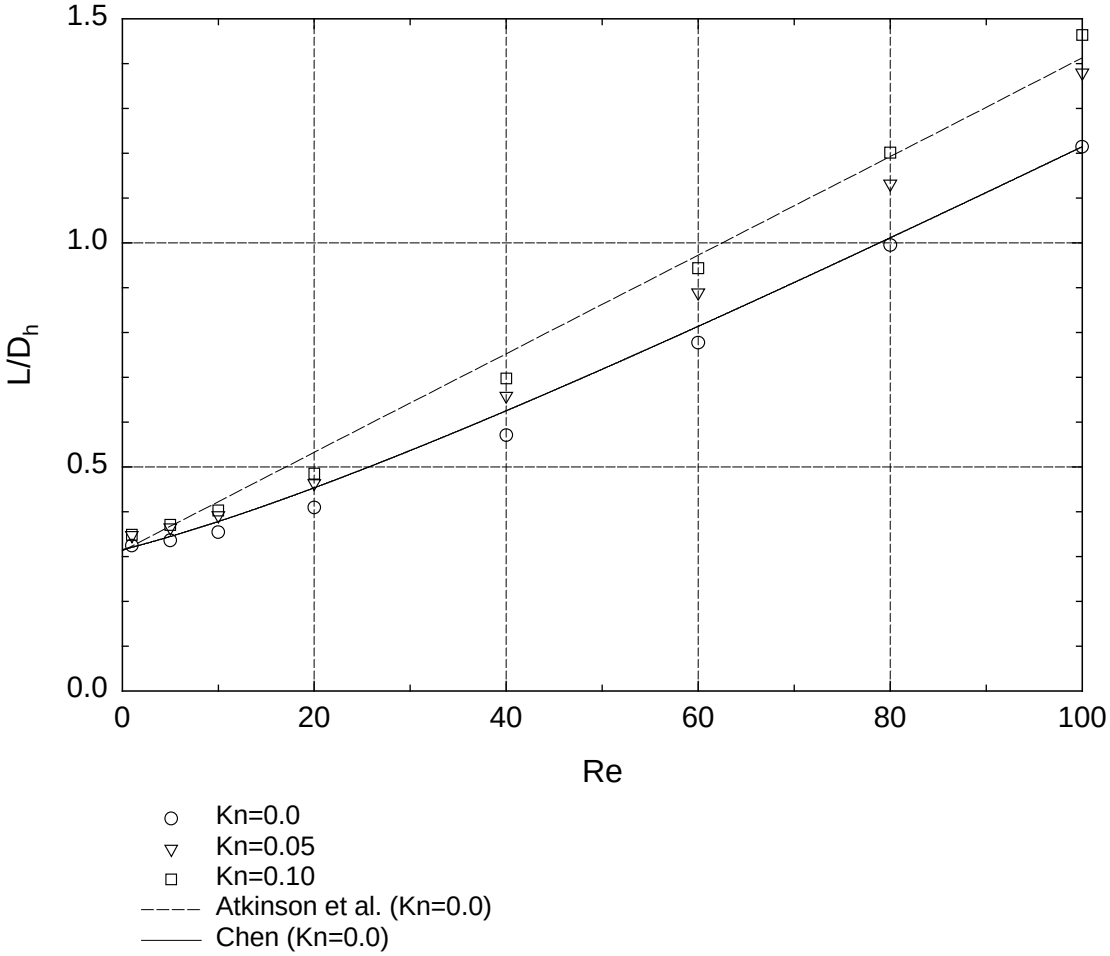

Figure 10: Detail of non-dimensionalised development lengths for flow between parallel plates (101×41 mesh)

Re	Kn=0.0	Kn=0.025	Kn=0.05	Kn=0.075	Kn=0.10
	L/D_h	L/D_h	L/D_h	L/D_h	L/D_h
1	0.3238	0.3389	0.3473	0.3495	0.3488
5	0.3360	0.3532	0.3646	0.3696	0.3703
10	0.3544	0.3776	0.3915	0.3999	0.4027
20	0.4092	0.4407	0.4636	0.4783	0.4849
40	0.5706	0.6168	0.6583	0.6841	0.6975
60	0.7769	0.8337	0.8892	0.9241	0.9436
80	0.9945	1.0619	1.1316	1.1762	1.2016
100	1.2141	1.2954	1.3795	1.4338	1.4640
150	1.7589	1.8808	2.0057	2.0846	2.1296
200	2.2966	2.4674	2.6340	2.7392	2.7994
250	2.8240	3.0528	3.2633	3.3951	3.4711
300	3.3425	3.6393	3.8916	4.0505	4.1447
350	3.8533	4.2235	4.5224	4.7083	4.8151
400	4.3555	4.8059	5.1509	5.3642	5.4898

Table 4: Non-dimensionalised development lengths for flow between parallel plates (101×41 mesh)

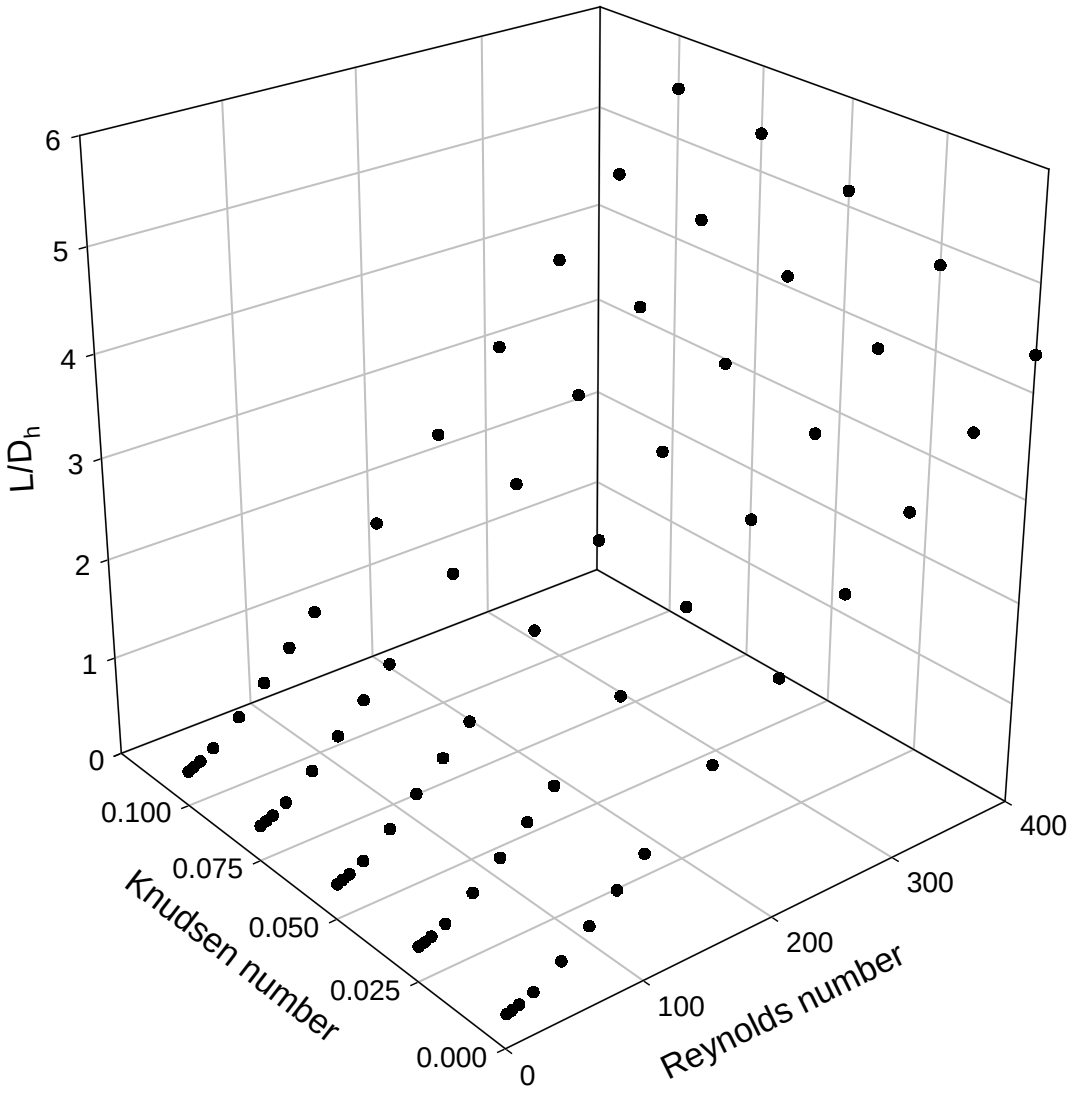

Figure 11: 3-dimensional representation of non-dimensionalised development lengths for flow between parallel plates

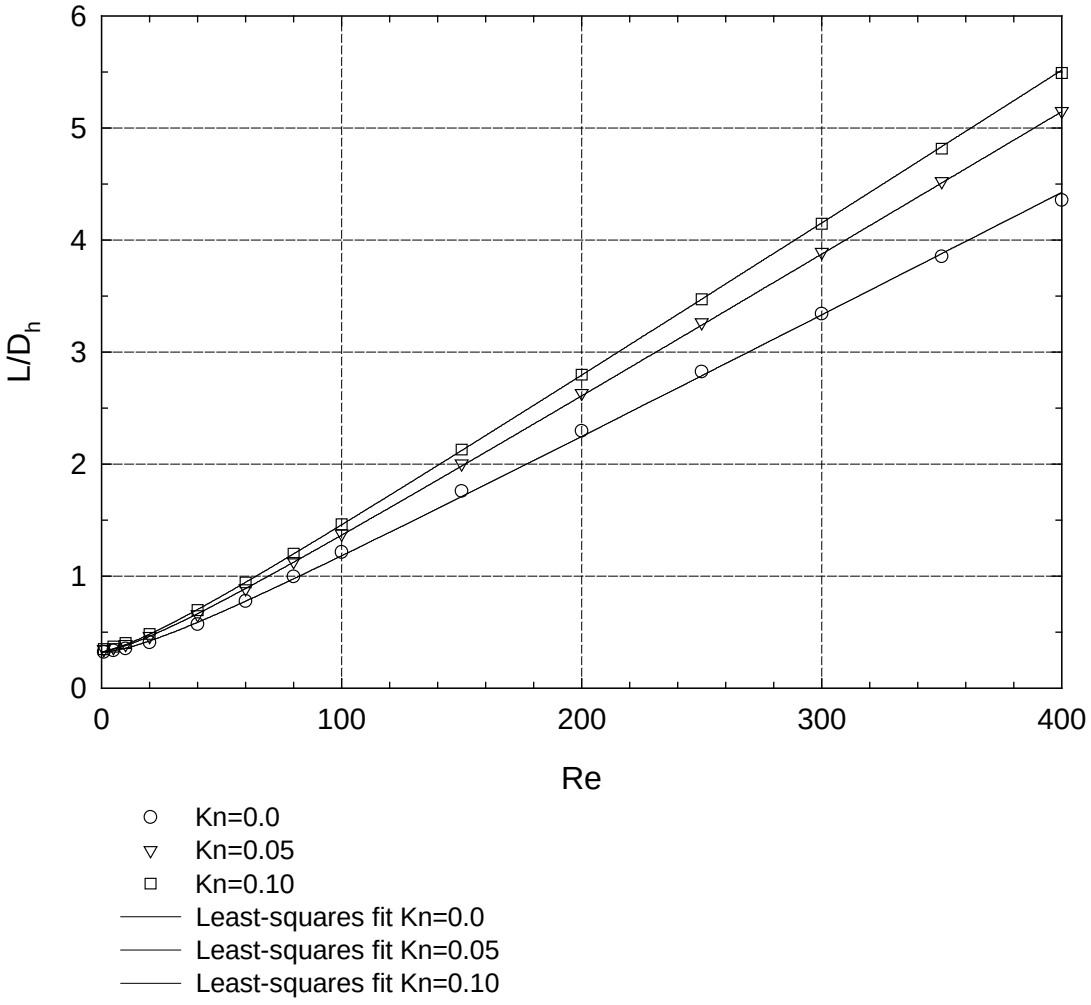

Figure 12: Least-squares surface fit of non-dimensionalised development lengths for flow between parallel plates